Assessment of Thermal Stresses in Asphalt Pavements Due to Environmental Conditions

Dr. C. Yavuzturk and Dr. K. Ksaibati
Department of Civil and Architectural Engineering
University of Wyoming
1000 East University Avenue, Dept. 3295
Laramie, WY 82071-3295

April 2006

Acknowledgement

This report has been prepared with funds provided by the United States Department of Transportation to the Mountain-Plains Consortium (MPC). The MPC member universities include North Dakota State University, Colorado State University, University of Wyoming, and Utah State University.

Disclaimer

Abstract

Temperature fluctuations in asphalt pavements significantly affect pavement stability and the selection of asphalt grading. Ability to accurately predict asphalt pavement temperatures at different depths and horizontal locations based on environmental conditions will greatly help pavement engineers not only in the selection of the asphalt grade to be used in various pavement lifts, but also in the accurate assessment of thermal stresses in and between various asphalt lifts. This is especially critical when the asphalt pavement is exposed to extreme freeze and thaw conditions. Accurate knowledge of the temperature and thermal stress distribution in asphalt pavements will allow for a more sophisticated specification of asphalt binder grades for lower lifts and thus provide an economical solution to rising pavement construction costs.

This report is Phase II of a previous MPC research project (MPC Report NO. 02-136) that developed a computer model using a transient, two-dimensional finite volume approach to mathematically describe the thermal response of asphalt pavements due to thermal environmental conditions on an hourly basis. The main objective of Phase II research is to expand the capabilities of the computer model to include the thermal effects of precipitation and to study the impact of the tilt angle from the horizontal of an asphalt pavement on asphalt temperature predictions. With the expanded capabilities of the computer model, it will be possible to develop preliminary thermal stress maps of asphalt pavements during seasonal and diurnal freeze/thaw cycles.

TABLE OF CONTENTS

LIST OF FIGURES

1. INTRODUCTION

Seasonal and diurnal fluctuations in ambient air temperatures, solar radiation, pavement materials and geometry, convective surface conditions, and precipitation significantly impact pavement stability and correspondingly the long-term success of pavement design. Accurate prediction of the temperature profile in pavements is critical in the assessment of pavement deflection, in back-calculations of pavement modulus values, in estimations of frost action and thaw onset, and in the assessment of diurnal and seasonal heating and cooling effects.

Ability to accurately predict asphalt pavement temperatures at different depths and horizontal locations based on thermal environmental conditions is of importance not only in the selection of the asphalt grade to be used in various pavement lifts, but also in the accurate assessment of thermal stresses in and between various asphalt lifts. This is especially critical when the asphalt pavement is exposed to extreme freeze and thaw conditions. Accurate knowledge of the pavement temperature profile coupled with the knowledge of thermal stress distribution allows for a more sophisticated selection of asphalt binder grades for various pavement lifts. Thus, lower grade less expensive binders may be specified for lower lifts where less temperature fluctuations are normally encountered and higher grade more expensive binders for lifts with significant temperature fluctuations. This distinction will provide an economical solution to rising pavement construction costs.

This report is Phase II of a previous MPC research project (MPC Report NO. 02-136, Yavuzturk and Ksaibati, 2002) that developed a computer model using a transient, two-dimensional finite volume approach to mathematically describe the thermal response of asphalt pavements due to thermal environmental conditions on an hourly basis.

The main objective of Phase II research is to expand the capabilities of the previously developed computer model to include the thermal effects of precipitation and to study the impact of the tilt angle from the horizontal of an asphalt pavement on asphalt temperature predictions. With the expanded capabilities of the computer model, it will be possible to develop preliminary thermal stress maps of asphalt pavements during seasonal and diurnal freeze/thaw cycles.

2. BACKGROUND AND LITERATURE SURVEY

An extensive literature review was conducted to survey research works previously performed to assess the effects of environmental conditions, specifically with respect to ambient air temperature fluctuations, on thermal stresses in pavements. The literature basically subdivides itself into two major areas of research. Significant amount of work has been presented on temperature distributions and thermal stresses in bridge decks. Even more research publications are found in thermal action of pavements not on bridge decks that is the focus of the research presented here. The literature survey provided below is complementary to the literature survey presented in Phase I of this project reported in Yavuzturk and Ksaibati (2002). Major relevant publications going back to the early 1990s are briefly discussed below:

Adkins and Merkley (1990) propose a numerical approach based on finite-difference modeling to assess temperature distributions in concrete pavements as a function of changes in thermal environmental conditions. The model attempts to predict the rate and depth of temperature changes during freeze and thaw cycles. The proposed model however does not model surface cooling effects due to precipitation, impact of surface tilt angle on surface boundary conditions and pavement internal thermal stresses due to varying temperature layers.

Stouffels et al. (1993) compare several computer programs for estimating asphalt concrete pavement temperatures. The study focuses on comparison between the results obtained from the FHWA integrated model and actual recorded pavement temperatures. The study determines that neglecting edge effects is not significant for typical pavement cross sections but may be important for shoulders and extreme cross sections.

Harik et al. (1994) develop an analysis technique to be used in conjunction with packaged finite element programs for the study of rigid pavements that are subjected to temperature loading. The pavement is idealized as a thin isotropic plate resting on a Winkler-type elastic foundation. Results obtained from simulations are presented and compared for both linear and non-linear temperature variations. The study concludes that temperature stresses in rigid pavement design may not be disregarded.

Choubane et al. (1995) provide an analysis and verification of thermal gradient effects on concrete pavements. An experimental and analytical study is presented to develop a method for determining realistic thermal-load induced stresses. The study concluded that the impact of the total temperature distribution throughout the depth of a concrete slab was more significant than the temperature differentials between the extreme slab fibers.

Ali and Lopez (1996) investigate relationships between climatic factors and pavement structural properties considering data collected under the Seasonal Monitoring Program of the Long-Term Pavement Performance Program. Correlations between pavement structural properties and climatic factors are studied using a series of statistical analyses.

Massad et al (1996) present a finite element study to investigate the effects of temperature variations and corresponding curling and thermal expansion stresses on plain-jointed concrete pavements. The three-dimensional model consists of four slabs separated by longitudinal and transverse joints. The model is used to perform parametric studies on curling and thermal expansion stresses that may develop at the joints and to study the influence of friction between slabs and the ground base. It is concluded that non-linear temperature distributions in slabs cause higher tensile stresses than linear distributions.

Shalaby et al. (1996) model the thermoelastic response of a multilayered pavement structure using a transient thermal analysis followed by a quasi-static stress analysis at discrete time-intervals using finite element analysis. The study conducts numerical analyses of two- and three-dimensional cracking problem. Based on a fracture mechanics approach, the potential of thermal cracks to propagate through the asphalt overlay is examined using both a displacement formula and energy balance principle. Also, the interaction between multiple cracks and the effect of bond between layers on crack propagation is investigated.

Yu et al. (1998) study the structural response of jointed plain concrete pavement slabs using data obtained from instrumented slabs constructed on existing asphalt concrete pavement on U.S. Interstate 70 near the Kansas-Colorado border. Curling deflections and through-thickness temperature profiles were measured. Analysis of the field data shows that the slabs had a considerable amount of built-in upward curling and that concrete slabs on a stiff base can act completely independent of the base or monolithically with the base depending on the loading conditions. The study also suggests that the effects of temperature gradients on the critical edge stresses may not be as great as previously assumed.

Pane et al. (1998) present a three-dimensional finite element analysis to assess the effects of non-linear temperature gradients in concrete pavements. The model is used to validate an analytical model proposed by Mohamed and Hansen (1996) to predict stresses in concrete pavements subjected to non-linear thermal gradients. The study investigates the condition of full contact for a non-linear thermal gradient that produces the maximum tensile strength.

Ionannides et al. (1998) study non-linear temperature and wheel load effects on multilayered concrete pavements considering a plate consisting of one or more layers, resting on a general elastic foundation. The resultant bending stress is presented as the sum of bending stresses due to applied loading and to an equivalent linear temperature gradient, plus the pure thermal stresses due to the non-linear part of the temperature distribution.

Nishizawa et al. (1998) provide a study on the prediction of thermal stresses in continuously reinforced concrete pavements. The analyses are based on measured data on actual test sections of continuously reinforced concrete pavements. The divides measured strains into axial, curling and non-linear components and examines each component. The study concludes that the curling component is predominant in terms of transverse stress, however, the maximum thermal stress is reduced by about 25% due to the non-linear component. A procedure is recommended for estimating the thermal stress.

Kuo (1998) suggests a numerical approach using a three-dimensional finite element analysis technique to develop a stress model in order to estimate pavement damage. Field temperature measurements obtained during different times of a day at 14 sites in the U.S. are input to calculate pavement compound stresses due to curling and wheel loads. An algorithm is developed to obtain equivalent damages and effective temperature differentials introducing a pavement fatigue hypothesis.

Liang and Niu (1998) present a closed-form analytical solution to determining slab temperatures in a three-layer pavement system that is subjected to a periodic variation of either the ambient air temperature or pavement surface temperature. The thermal analysis is coupled with a plate theory with Winkler foundation to allow for the calculation of curling stresses and bending moments. The analyses show that the pavement temperature distributions can be highly non-linear especially when the ambient air temperatures fluctuate as a function of time. The study concludes that the frequency of temperature variations rather than the amplitude has the most significant impact on calculated temperature profiles thus thermal stresses in pavements.

Boutin and Lupien (2000) present an analysis of factors affecting asphalt cracking using observations and correlations from several Canadian test samples. A prediction model is presented to evaluate thermal cracking over time. They concluded that criteria derived from penetration tests are good indicators of thermal cracking susceptibility of asphalt binders. Temperature, thickness of asphalt, and characteristics of the binder all determine if the pavement will crack or not. Other factors like characteristics of aggregates, pavement age, width of asphalt pavement, friction between asphalt pavement and base course have an effect on the severity of thermal cracking when a susceptible asphalt binder is used. Temperature in the middle of the asphalt pavement should be used to design asphalt pavement to resist thermal cracking.

Anderson et al. (2001) present thermal cracking temperatures and corresponding ranking for 42 plain and modified asphalt binders. The study compares the thermal cracking temperatures by the original and modified Superpave specifications (that takes into account measured stiffness and tensile strength of the binder to determine the thermal cracking temperature). The analyses are based on 14 asphalt binders of known fracture properties and produced from a common base material.

Shen and Kirkner (2001) present a parameter study on factors contributing to thermal cracking of asphalt pavements. A semi-analytical model was developed to account for multiscale nature of thermal cracking of asphalt-concrete pavements, including the effects of viscoelasticity. The study showed the most important parameters to be material homogeneity, ductility, frictional constraint on the interface, and rate of cooling.

3. OBJECTIVE OF THE STUDY

The objective of this study is two-fold:

1) The transient, two-dimensional finite difference model of a multilayered pavement slab reported in Yavuzturk and Ksaibati (2002) is expanded and improved to include the effects of pavement surface tilt angle and the pavement surface cooling effects due to precipitation. The improved model will be capable of more accurate temperature predictions in pavement slabs.

2) A module is added to the model that is capable of providing thermal stress estimations in multilayered pavement slabs due to thermal environmental conditions. It will thus be possible to develop preliminary thermal stress maps of asphalt pavements during seasonal and diurnal freeze/thaw cycles.

4. METHODOLOGY

The two-dimensional finite-difference approach used to predict temperatures in asphalt pavements is described in detail below:

4.1 Energy Balance in Pavements

The temperature profile in an asphaltic pavement is directly affected by the thermal environmental conditions to which it is exposed. The primary modes of heat transfer are incident solar radiation, thermal and long-wave radiation between the pavement surface and the sky, convection due to heat transfer between the pavement surface and the fluid (air or water) that is in contact with the surface, and conduction inside the pavement.

The intensity of solar radiation (direct and diffuse) is dependent on diurnal cycles, the location of the sun in the sky and the incident angle between the surface and sun's rays. The solar radiation results in direct and diffuse heat gain on the pavement through absorption of solar energy by the pavement. The convection heat flux is a function of fluid velocity and direction, and it is primarily affected by wind velocity and direction upon the surface. As the convection heat transfer coefficient increases due to higher velocities and opportune wind directions, the convective heat flux also increases. Thus, at relatively high wind velocities, a convective cooling of the surface occurs when the temperature of the wind is lower than the temperature of the pavement surface. The direction of the heat transfer due to thermal and long-wave radiation is away from the pavement since deep sky temperatures are typically significantly lower than pavement surface temperatures.

The surface energy balance on a pavement requires that the sum of all heat gains through the surface of the pavement must be equal to the heat conducted in the pavement. The direction of the heat flux due to convection and thermal radiation is a function of the temperature difference between the pavement surface and the bulk fluid/sky temperatures. In cases where the sky temperature and the bulk fluid temperature are lower than the pavement surface temperature, a cooling of the surface occurs while the surface might simultaneously be heated through incident solar radiation. Thus, depending on the magnitudes of individual heat fluxes, a heating or a cooling of the pavement takes place. An adiabatic bottom surface can be assumed for sufficiently thick pavements stipulating no heat transfer between the pavement and sub-grade layers. Similarly, side surfaces of the pavement (pavement edges) are considered to be adiabatic for sufficiently large horizontal expansions since spatial temperature changes in the vertical direction will be much greater than horizontal changes at pavement edges, and any heat transfer through pavement edge surfaces can be neglected.

The details of the numerical model used in this study may be found in Yavuzturk and Ksaibati (2002), as this report is the result of second phase of MPC research project 02-136.

However, a detailed discussion of numerical model improvements is provided below. Three new capabilities have been added: a) A module to allow for non-horizontal pavement surfaces (surface tilt angle); b) A module to calculate the effects of precipitation; c) A module to estimate thermal stresses due to non-linear thermal loading of the pavement slab.

4.2 Model Improvements to Include Tilt Angle

A new FORTRAN module was developed to expand the capabilities of the current numerical model to handle effects of the tilt angle of a pavement slab on the incident solar radiation. In so doing, it became necessary to account for the wide variety of formats in which solar data may be available to a user. Therefore, the new module was developed in a general sense to process solar data, depending on the format. These formats include:

(1) *Typical meteorological year (TMY) or equivalent data available.* In this case, solar radiation data are usually available in terms of beam and diffuse components. The new FORTRAN module reads these data from a file and then computes total solar radiation on a surface of arbitrary orientation.

(2) *No solar radiation data available*. In this case, the model computes total theoretical solar radiation on a surface of arbitrary orientation at a particular location as a function of latitude, longitude, atmospheric clearness, and pavement surface orientation.

(3) *Total horizontal radiation available.* In this case, the solar data available is sufficient only if the pavement surface is horizontal. If the surface to be modeled is not horizontal, the solar radiation data must be split into its beam and diffuse components and then recombined with the proper solar angle of incidence.

The output provided by the new solar module is total solar radiation on an arbitrary surface. The user is then responsible for transferring the data into the weather file, and then the numerical model uses the solar data in the energy balance calculations as before.

4.2.1 Mathematical Description

4.2.1.1. Calculation of the Solar Incidence Angle

Several calculations are needed to compute the solar incidence angle. The hourly solar incidence angle (θ) is defined as the angle between the beam radiation on a surface and the normal to that surface. It is important in calculating the total hourly solar radiation on a surface (I_t):

$$I = I_b \cos\theta + I_d \qquad (1)$$

where: I is the total solar radiation on a surface (W/m^2); I_b is the beam radiation (W/m^2), θ is the solar angle of incidence; and I_d is the diffuse radiation (W/m^2). Beam radiation is defined as radiation received from the sun without having been scattered by the atmosphere. Diffuse radiation is defined as the solar radiation received from the sun after its direction has been changed by scattering by the atmosphere.

The first step in computing the solar angle of incidence is to compute the solar time. The local solar time (*LST*) is computed from the local civil time (*LCT*) using a quantity known as the equation of time (*EOT*), which corrects for the perturbations in the earth's rate of rotation. The LCT is computed by:

$$LCT = ST + 4 \times (Meridian - Long) \qquad (2)$$

where: *ST* is the standard time, *Meridian* is the standard meridian at the location, and *Long* is the longitude of the location. The *LST* is then computed by:

$$LST = LCT + \frac{EOT}{60} \tag{3}$$

where EOT is given by Spencer (1971) as:

$$EOT = 299.2\begin{pmatrix} 0.000075 + 0.001868\cos N - 0.032077\sin N - \\ 0.014615\cos 2N - 0.04089\sin 2N \end{pmatrix} \tag{4}$$

where N is a correction for the day of the year (n) given by:

$$N = (n-1)\frac{360}{365} \tag{5}$$

Several solar angles are needed for computation of the solar incidence angle. First, the declination angle (δ) is computed, which is the angular position of the sun at solar noon with respect to the plane of the equator. This is computed after Spencer (1971) as:

$$\begin{aligned} \delta = {} & 0.39637 - 22.91327\cos N + 4.02543\sin N - 0.3872\cos 2N \\ & + 0.05197\sin 2N - 0.15453\cos 3N + 0.0848\sin 3N \end{aligned} \tag{6}$$

where N is as described in Equation 5. Next, the hour angle (h) is computed, which is the angular displacement of the sun east or west of solar noon due to rotation of the earth on its axis at 15^o per hour:

$$h = 15|12 - LST| \tag{7}$$

The solar altitude angle (β), the angle between the horizontal and a line to the sun, is now given by:

$$\beta = \sin^{-1}\left[\cos(L)\cos(h)\cos(\delta) + \sin(L)\sin(\delta)\right] \tag{8}$$

where L is the latitude of the location. The solar azimuth angle (ϕ), taken positive when west of south, is given by:

$$\phi = \cos^{-1}\left[\frac{\sin(\beta)\sin(L) - \sin(\delta)}{\cos(\beta)\cos(L)}\right] \tag{9}$$

The surface solar azimuth (γ) is next computed as:

$$\gamma = \phi - \varphi \tag{10}$$

where φ is the surface azimuth in degrees west of south. Finally, the solar incidence angle (θ) is computed as:

$$\theta = \cos^{-1}\left[\cos(\beta)\cos(\gamma)\sin(\alpha) + \sin(\beta)\cos(\alpha)\right] \tag{11}$$

where α is the tilt angle of the surface.

4.2.1.2. Calculation of Beam and Diffuse Solar Radiation

In cases where solar radiation data are not accessible, methods are available for computation of theoretical solar radiation (ASHRAE, 2001; Duffie and Beckman, 1991). The solar constant is the rate of extraterrestrial irradiation received on a unit area of surface perpendicular to the direction of propagation of the radiation, outside of the earth's atmosphere (Duffie and Beckman, 1991). The value of the mean solar constant is approximately 1367 W/m^2.

ASHRAE (2001) describes a model (known as the ASHRAE Clear Sky Model) for computing solar irradiation at the earth's surface by applying corrections to the solar constant. The normal direct irradiation (G_{ND}) (also referred to as the beam radiation) in units of W/m^2 is given by:

$$G_{ND} = \frac{A}{\exp\left(B \big/ \sin\beta\right)} \tag{12}$$

where A is the apparent solar irradiation at air mass equal to zero (W/m^2) and B is the atmospheric extinction coefficient. The values of the A and B coefficients are time-dependent, varying over the annual cycle.

The direct radiation (G_d) in units of W/m^2 on a surface of arbitrary orientation is given by:

$$G_D = C_N G_{ND} \cos\theta \tag{13}$$

where C_N is the clearness number, which ranges from 0.90 for humid climates to 1.10 for high altitude climates. The diffuse radiation (G_d) in units of W/m^2 is given by:

$$G_d = \frac{C\, G_{ND}}{C_N{}^2} \tag{14}$$

where C is the ratio of diffuse irradiation on a horizontal surface to direct normal irradiation. The value of the C coefficient is time-dependent, varying over the annual cycle.

Finally, the total solar radiation on the surface is found by summing G_D and G_d.

4.2.1.3. Splitting of Horizontal Solar Radiation into Beam and Diffuse Components

In some cases, pavement designers may have total horizontal radiation data, but the surface in question may not be horizontal. This is the case for the LTTP data from Alabama, Delaware, and Virginia, where it is desirable to examine effects of the tilt angle on the pavement surface temperature. There are a few methods available for splitting solar radiation into its respective components, but the best methods are not fully settled (Duffie and Beckman, 1991).

The present methods for estimating the beam and diffuse components of solar radiation are based on empirical measurements. The usual approach has been to correlate the ratio I_d/I to k_t, where I_d is the hourly diffuse solar radiation (W/m^2), I is the measured hourly total solar radiation on a horizontal surface (W/m^2), and k_t is the hourly clearness index, defined as the ratio I/G_{ND}, where G_{ND} is given by Equation 12. Correlations given by Duffie and Beckman (1991) are:

$$\frac{I_d}{I} = \begin{pmatrix} 1.0 - 0.249k_T & ,0.00 < k_T \le 0.35 \\ 1.557 - 1.84k_T & ,0.35 < k_T \le 0.75 \\ 0.177 & ,0.75 < k_T > 1.00 \end{pmatrix} \quad (15)$$

To apply Equation 15, k_T is computed using the given or measured total radiation on a horizontal surface. Based on the value of k_T, the appropriate correlation is used to find I_d. The beam radiation (I_b) can then be found using Equation 1, and new I values can be computed for any values of the incidence angle (θ).

4.2.2. Computer Implementation and Description of Simulations Performed

As mentioned above, a new FORTRAN module was developed to handle the solar calculations. Output from the solar module is total radiation on an arbitrary surface. The user is responsible for transferring the solar module output to the weather file, which is read by the pavement model as before. The solar module input data are summarized below:

```
STARTDAY        =     START DAY OF CALCULATIONS (1-365)
ENDDAY          =     END DAY OF CALCULATIONS (1-365)

DESCRIPTION OF LOCATION:
     LAT        =     LATITUDE OF LOCATION (degrees)
     LONG       =     LONGITUDE OF LOCATION (degrees)
     MERIDIAN   =     STANDARD MERIDIAN OF LOCATION (degrees)
     CN         =     ASHRAE CLEARNESS NUMBER (-)

DESCRIPTION OF SURFACE:
     ALPHA      =     TILT ANGLE OF SURFACE (degrees)
     PSI        =     SURFACE AZIMUTH (degrees W of S)

CALCULATION PARAMETERS:
     SOLARFLAG  =  1 for calculation of beam & diffuse
                <> 1 if beam & diffuse are provided
```

The solar module in conjunction with the existing pavement model were used to examine the effects of pavement tilt on the Alabama, Delaware, and Virginia LTTP data described in the previous report (Yavuzturk and Ksaibati, 2002). Beam and diffuse components were derived from measured total radiation on horizontal as described above in Section 4.2.1.3. For each data set, the solar module was used to compute solar radiation on a pavement slab oriented at azimuths of north, south, east, and west with tilt angles of 0^o, 2.5^o, 5^o, and 7.5^o from the horizontal. Therefore, for each of the 3 locations, 16 simulations were performed. Goodness of fit between the measured and modeled data was computed using the sum of squared residuals.

4.3. Model Improvements to Include Precipitation

The existing pavement model was expanded to include heat transfer effects from precipitation. Two additional heat transfer processes were considered due to precipitation: advection and evaporation.

4.3.1. Mathematical Description

Advection refers to the process of heat transfer due to falling rain and its temperature difference between the pavement surface, and is given by:

$$q''_{rain} = (3.6x10^{-6})\dot{v}\rho c_p (T_{rain} - T_{surface}) \tag{16}$$

where q''_{rain} is the heat flux due to falling rain (W/m^2), $\dot{v}$ is the rainfall rate (mm/hr), ρ is the density of rain water (kg/m^3), c_p is the specific heat capacity of rain water (J/(kg-^{o}C)), and T is the temperature. Accumulation of rain is not considered; rainfall is assumed to drain instantaneously from the pavement surface, forming a thin film from which evaporation occurs.

Evaporation is the more important heat transfer mechanism contributing to slab cooling. First, the j-factor analogy is used to compute the mass transfer of evaporating water ($\dot{m}''_w$) at the slab surface:

$$\dot{m}''_w = h_d (w_{air} - w_{surface}) \tag{17}$$

where h_d is the mass transfer coefficient (kg/s-m^2), w_{air} is the humidity ratio of the ambient air (kg water/kg dry air), and w_{surf} represents the humidity ratio of saturated air at the slab surface. The w_{surf} term is computed using correlations given by ASHRAE (2001). The mass transfer coefficient (h_d) is defined using the Chilton-Colburn analogy as:

$$h_d = \frac{h_c}{c_p \mathrm{Le}^{\frac{2}{3}}} \tag{18}$$

where h_c is the convection coefficient (W/m-^{o}C) described in the previous report (Yavuzturk and Ksaibati, 2002), c_p is the specific heat capacity of the air (J/kg-^{o}C) evaluated at the slab-air film temperature, and Le is the Lewis number. Le is computed as:

$$\mathrm{Le} = \frac{\alpha}{D_{AB}} \tag{19}$$

where α is the thermal diffusivity of the air (m^2/s) evaluated at the slab-air film temperature and D_{AB} represents the binary diffusion coefficient. The thermal properties (α and c_p) of air are computed at each time step using correlations given by Irvine and Liley (1984). D_{AB} is computed after Mills (1995) who references Marrero and Mason (1972):

$$D_{AB} = \frac{1.87x10^{-10} T^{2.072}}{P_{air}} \qquad (280\mathrm{K} < \mathrm{T} < 450\mathrm{K}) \tag{20}$$

where T refers to the slab-air film temperature in absolute units and P_{air} is the atmospheric pressure in atmospheres. The heat flux due to evaporation ($q''_{evaporation}$) is then computed by:

$$q''_{evaporation} = h_{fg} \dot{m}''_{w} \tag{21}$$

where h_{fg} is the latent heat of vaporization and is computed from the relationship given by Irvine and Liley (1984).

4.3.2. Computer Implementation and Description of Simulations Performed

The above mathematical descriptions were added to the pavement FORTRAN model. Two new weather parameters are required in the weather file: hourly rainfall rate and hourly humidity ratio. Values of the humidity ratio are usually included in typical meteorological year (TMY) data sets discussed in section 4.5. Hourly rainfall data, however, must be obtained from local weather records; the concept of "typical" hourly rainfall rates does not exist.

To examine the effects of rainfall on slab surface temperature, the model was executed with weather data for the month of May from the Cheyenne, WY, TMY data set. Rainfall rates were randomly generated per hour and range from 0 to 1 mm/hr. (Figure 1). The monthly total was 323.4 mm (12.7 in.), which although unrealistically high, was sufficient for examining rainfall effects on slab surface temperature.

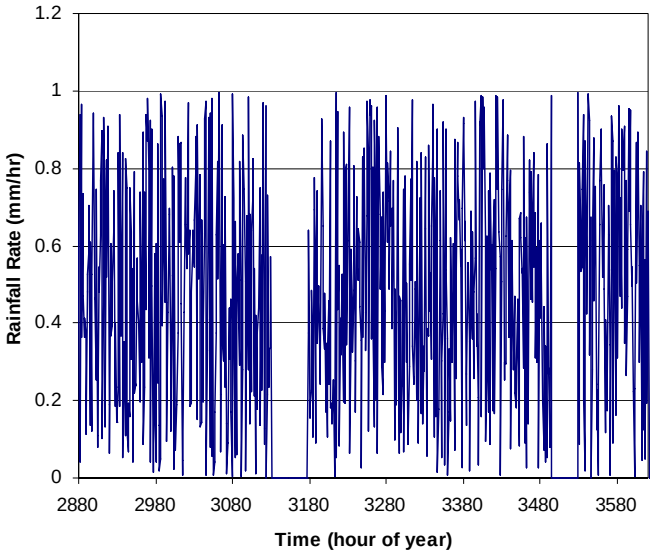

Figure 1. Randomly generated rainfall rates for use in examining rainfall effects on slab surface temperature

4.4. Model Improvement to Include Thermal Stress Estimations

It is well-known that thermal cracking of asphalt pavement is associated with low temperatures. Cold conditions induce shrinkage and the formation of tensile stresses in the pavement materials, which in turn results in fracture when the tensile strength of the asphalt is exceeded. Calculation of thermal stresses in asphalt pavements is complicated by the fact that it behaves as a visco-elastic material. The modulus of elasticity (E) of asphalt is a temperature-dependent property, and at very low temperatures, bitumen takes on a brittle character. Several researchers have attempted to estimate cracking temperatures in asphalt pavement with empirical approaches. The difficulty lies in adequately mathematically describing the rheological properties of a bituminous mixture.

The thermal stress model incorporated into the pavement model is that described by Hills (1974):

$$\sigma_{th} = c\alpha_{th}\Sigma S\Delta T \tag{22}$$

where σ_{th} is the thermal stress (MPa), α_{th} is the coefficient of thermal contraction ($^{o}C^{-1}$), S is the stiffness modulus (MPa), ΔT is the temperature change over the time interval of concern, and c is a coefficient that adjusts the thermal stress based on the constraint geometry of the slab (i.e. plane constraint, linear constraint, fixed end beam). Note that $\alpha_{th}\Delta T$ is the thermal strain.

The stiffness modulus (S) used in the stress model is similar to the modulus of elasticity, except that it is dependent on temperature and time of loading. Therefore, it is particularly suitable for describing visco-elastic materials, which exhibit both elastic behavior (where strain is independent of time) and viscous behavior (where strain is dependent on time of loading). The summation of $S\Delta T$ over time, as employed in the Hills (1974) model, accounts for the stress history. The usual method of determining the stiffness modulus is through nomographs originally published by Shell Oil Company, based on 20 years of laboratory work.

4.4.1. Computer Implementation and Description of Simulations Performed

The above mathematical descriptions of thermal stress were added to the pavement FORTRAN model. Stresses are computed on hourly intervals. New input data required by the user are the coefficient of thermal expansion, c coefficient in Equation 22, and the stiffness modulus at corresponding high and low temperatures (stiffness is typically determined at 25^{o}C and –40^{o}C). The model performs a logarithmic curve fit to determine the stiffness at intermediate temperatures (note Figure 4)

Sets of single and double test section lane simulations were conducted. For computational efficiency, single-lane test sections are scaled to a width of 1 m and the double-lane test sections are scaled to a width of 2 m. The scaling of pavement slab widths is appropriate since adiabatic pavement edges are stipulated in the numerical model (Yavuzturk and Ksaibati 2002) and the nature of the heat transfer phenomena does not change in the horizontal direction for homogeneous material properties.

Pavement slab geometries and spatially varying thermal conductivities are shown for each case in Figures 2 and 3. The purpose of the single test lane simulations was to observe the effects of vertically varying thermal properties on stresses. A base case is established representative of a pavement of two layers that are relatively similar with respect to thermal properties of typical lifts. Cases 1 and 2 are representative of an asphalt slab with low thermal conductivity surface and high thermal conductivity surface, respectively. The purpose of the double test lane simulations was to observe the effects of horizontally varying thermal properties on stresses (Cases 3 and 4).

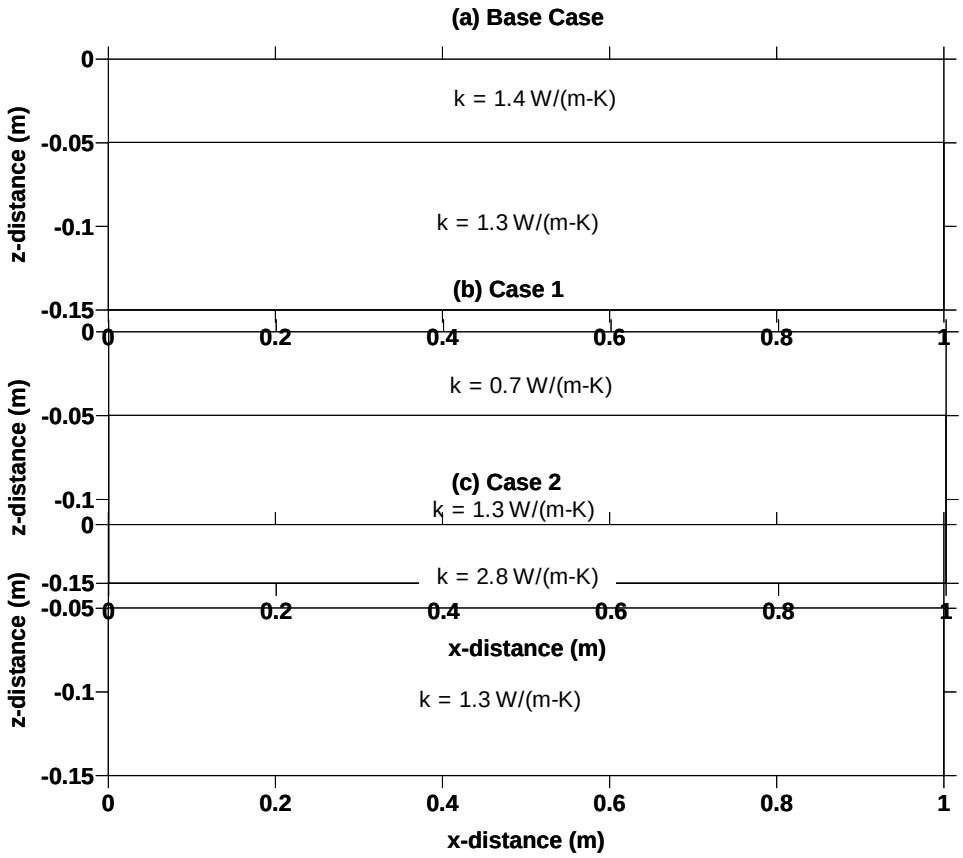

Figure 2. Model input spatial data for single-lane test cases.

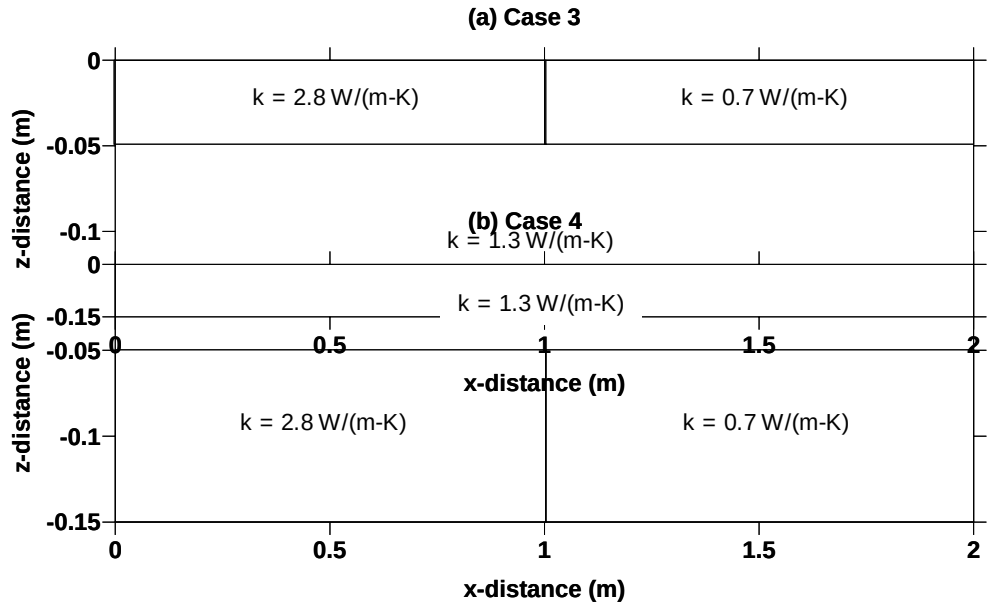

Figure 3. Model input spatial data for two-lane test cases

The model input data for the stress simulations were as follows:
Grid data:

- Grid spacing = 0.025 m
- Time step = 300 s

Thermal Property data:

- Thermal emissivity = 0.95
- Absorptivity: = 0.99
- Volumetric heat capacity: = 1900 kJ/(m^3-K)
- Coeff. of thermal contraction: = 2.0E-4 $^oC^{-1}$
- c coefficient: = 1.33 (infinite slab from Hills (1974)

Values of the stiffness modulus were determined from nomographs and data given by Hills (1974) and Yoder and Witczak (1975). These are plotted versus temperature in Figure 4. Based on data given by Hills (1974), the tensile strength of asphalt is taken as 0.5 MPa, and therefore, this is the critical value used to determine whether or not simulated asphalt pavements will crack.

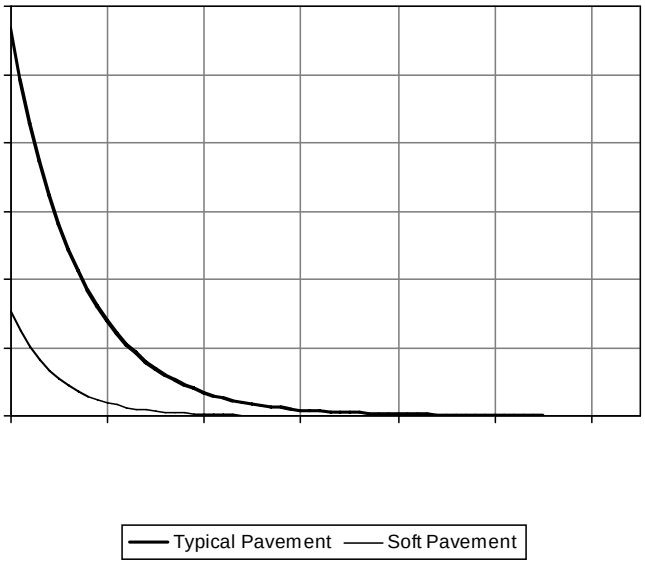

Figure 4. Stiffness moduli versus temperature for simulated typical and soft asphalt pavement

4.5. Climate and Pavement Data

SHRP and LTPP climate and pavement data have been used for the assessment of the asphalt surface tilt angle on pavement temperatures. The data were extracted from the data archives of the Seasonal Monitoring Program (SMP) conducted under the Long-Term Pavement Performance Program. The SMP established a number of data collection sites in the United States and Canada to evaluate the thermal seasonal response of asphaltic pavements. These sites included weather stations and pavement temperature sensors to log climate and pavement data on an hourly basis.

For the impact of precipitation and thermal stress estimation, typical meteorological year (TMY) weather data were input. A Typical Meteorological Year (TMY) weather data file is a data set of hourly values of solar radiation and meteorological elements for a one-year period. It consists of months selected from individual years and summarized to form a complete year and provides a standard for hourly data for solar radiation and other meteorological elements. The TMY weather file represents conditions judged to be typical over a long period of time, such as 30 years.

The TMY weather files were derived from the National Solar Radiation Data Base (NSRDB), which was completed by the National Renewable Energy Laboratory (NREL). The NSRDB accounts for any recent climate changes and provides more accurate values of solar radiation due to a better model for estimating values (More than 90% of the solar radiation data in both data bases are modeled), more measured data including direct normal radiation, improved instrument calibration methods, and rigorous procedures for assessing quality of data. The TMY weather files were created using similar procedures that were developed at Sandia National Laboratories by Hall et al. (1978). For example, in the case of the NSRDB, which contains 30 years of data, all 30 Januarys are examined, and the one judged most typical is selected to be included in the TMY. The other months of the year are treated in a like manner, and then the 12 selected typical months are concatenated to form a complete year. The 12 selected typical months for each station were chosen from statistics determined by using five elements: global horizontal radiation, direct normal radiation, dry bulb temperature, dew point temperature, and wind speed.

5. SIMULATION RESULTS AND DISCUSSION

5.1. Model Improvements to Include Tilt Angle

Contours of the sum of squared residuals of measured and modeled pavement surface temperature (normalized to the base cases) are shown in Figure 5 for the LTTP data. In all cases, a better match of modeled to measured data was found by tilting the pavement surface. For the Alabama data set, the lowest sum of squared residual (0.92) was found at a pavement orientation tilted west at an angle of 7.5^{o} from the horizontal. For the Delaware data set, the lowest sum of squared residual (0.93) was also found at a pavement orientation tilted west at an angle of 7.5^{o} from the horizontal. For the Virginia data set, the lowest sum of squared residual (0.94) was found at a pavement orientation tilted west at an angle of 2.5^{o} from the horizontal.

The interpretation of the above results is somewhat ambiguous, since the actual orientation of the test pavement section and its exposure to solar radiation are unknown. However, a more useful analysis would be to examine the effect of the tilt angle on the pavement surface temperature in a general sense. Figures 6-8 show (for clarity) maximum and minimum pavement surface temperatures for the Bismarck, ND, Cheyenne, WY, and Phoenix, AZ, typical meteorological year data sets and for a pavement surface facing major polar orientations tilted at 7.5° from the horizontal. A review of these figures shows the impact of the tilt angle on the pavement surface temperatures, specifically when the surface is tilted to the south, pavement surface temperatures may be significantly higher. The analyses indicate that the pavement surface temperature differentials are greater in the winter months than in the summer months.

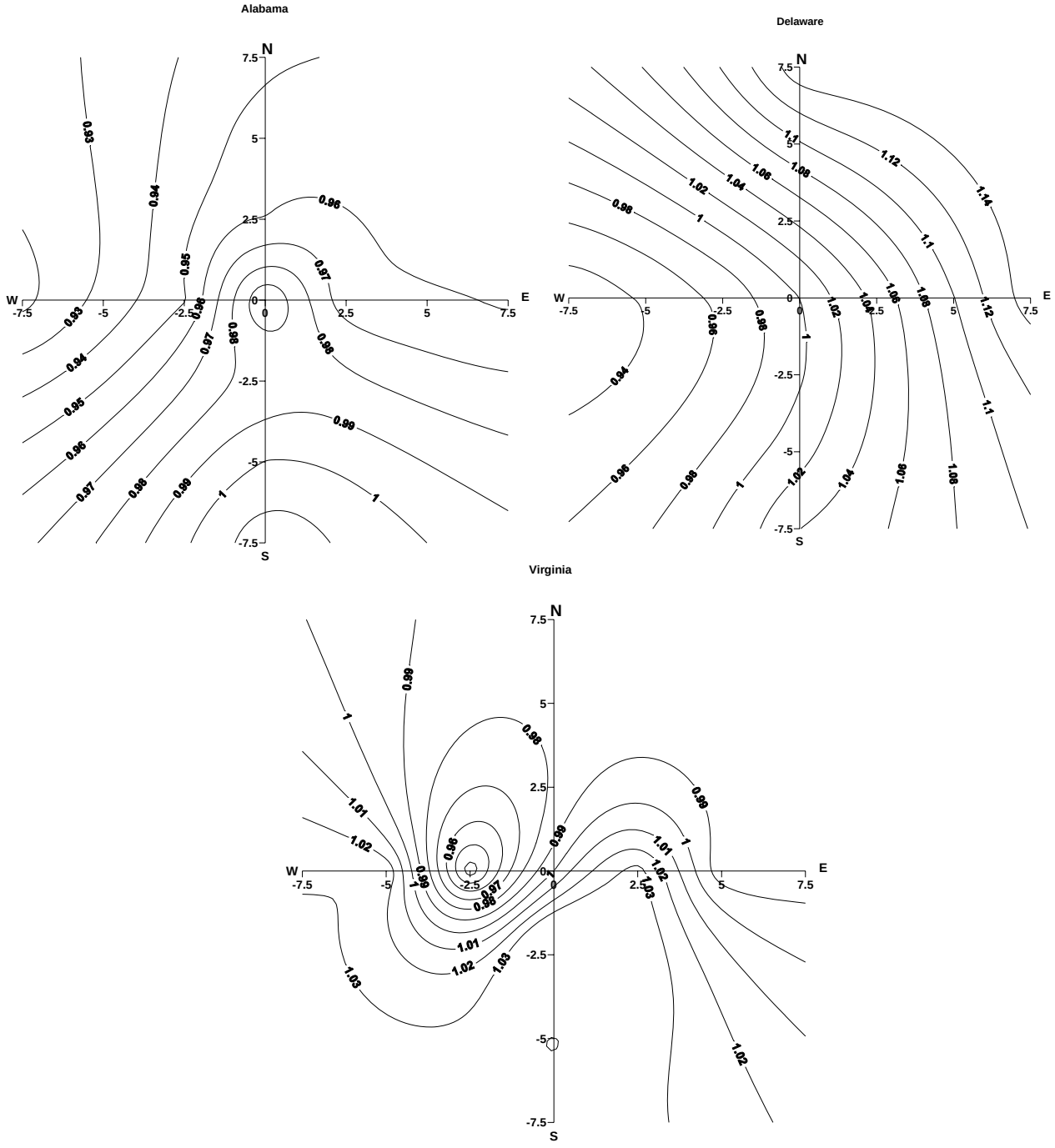

Figure 5. Contours of Σ (residuals)^2 normalized to base cases (no tilt) for Alabama, Delaware, and Virginia LTTP data. The axes represent azimuth direction of pavement section with values of the tilt angle.

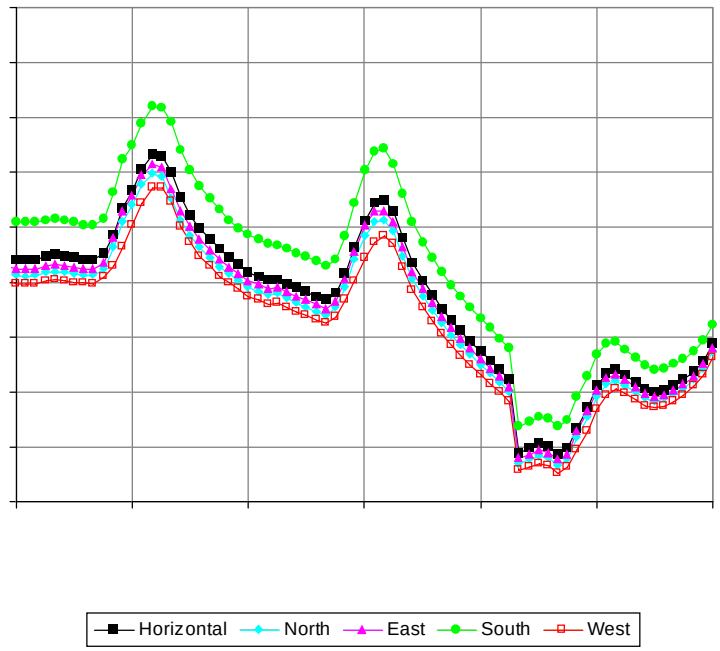

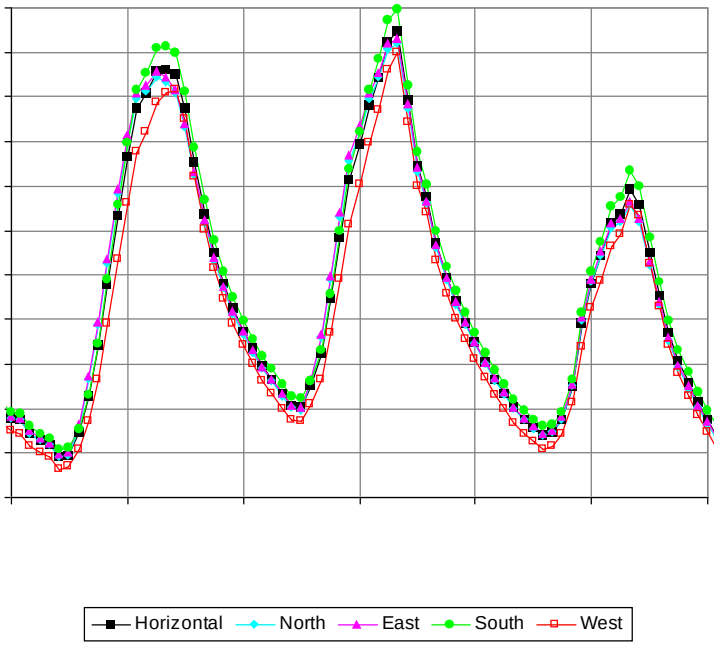

Figure 6. Comparison of hourly pavement surface temperatures for a three-day period containing the hour of **(a)** minimum occurrence and **(b)** maximum occurrence for the Bismarck, ND, TMY data set for a horizontal pavement surface and for a pavement surface tilted 7.5^{o} facing north, east, south, and west.

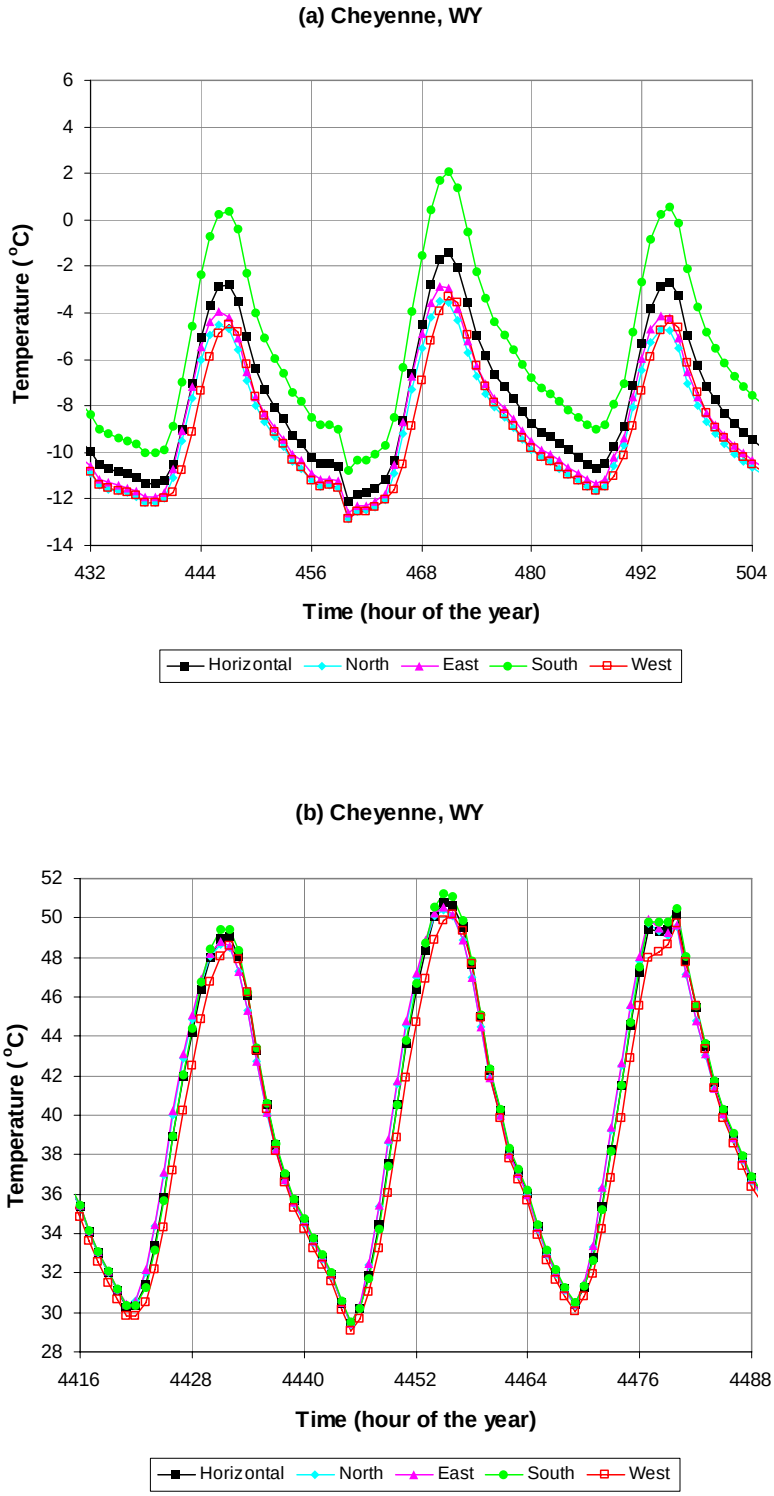

Figure 7. Comparison of hourly pavement surface temperatures for a three-day period containing the hour of **(a)** minimum occurrence and **(b)** maximum occurrence for the Cheyenne, WY, TMY data set for a horizontal pavement surface and for a pavement surface tilted 7.5° facing north, east, south, and west

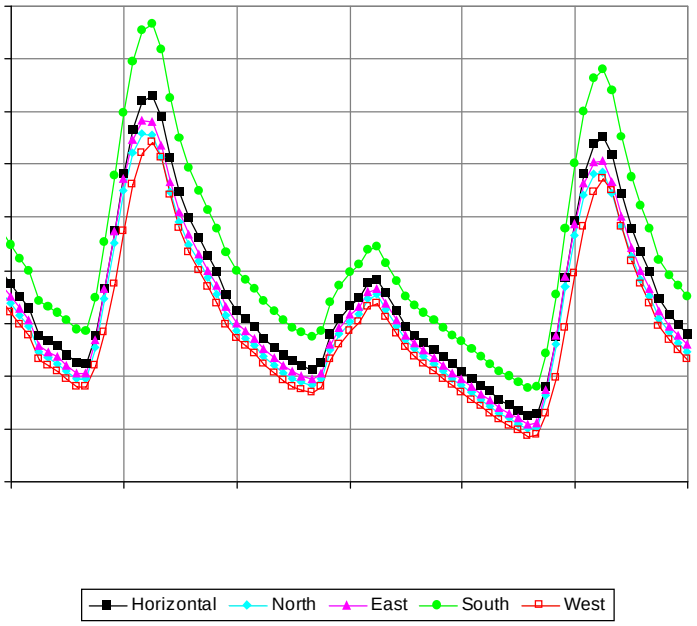

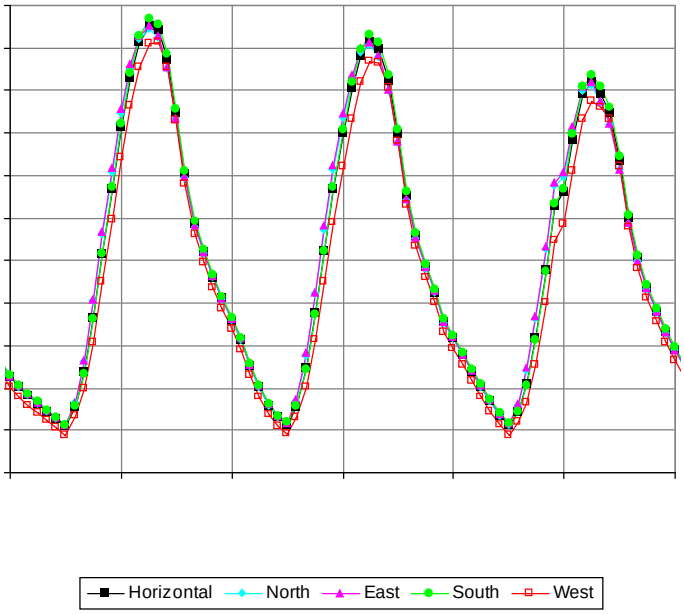

Figure 8. Comparison of hourly pavement surface temperatures for a three-day period containing the hour of **(a)** minimum occurrence and **(b)** maximum occurrence for the Phoenix, AZ, TMY data set for a horizontal pavement surface and for a pavement surface tilted 7.5^{o} facing north, east, south, and west.

5.2 Model Improvements to Include Precipitation

The simulations considering precipitation of rain were conducted using a rainwater temperature that is equal to the temperature of the air. The stipulation is somewhat conservative for summer months as depending on the climatic region during summer rainwater temperature is typically lower than the air temperature. In winter months, a convergence of rainwater and air temperatures is more likely.

Pavement surface temperatures with simulated precipitation are shown in Figure 9 for the month of May for Cheyenne, WY. The addition of precipitation and subsequent evaporation provides a significant cooling effect on the pavement surface, with temperatures observed to be on the order of 5-10^{o}C cooler with precipitation and evaporation included.

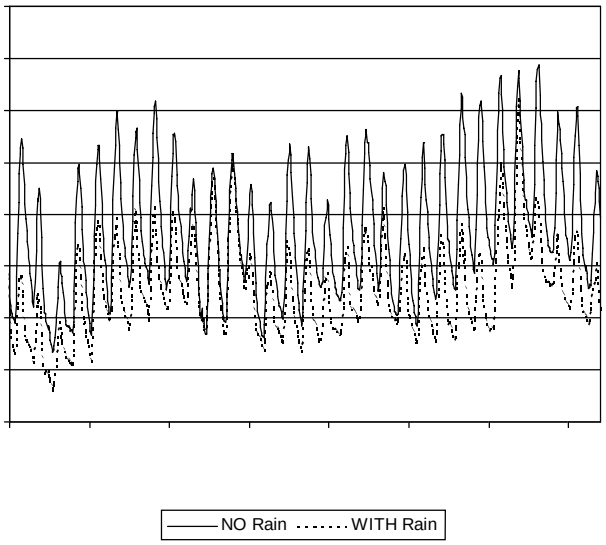

Figure 9. Slab top surface temperature with and without simulated rainfall for Cheyenne typical meteorological data for the month of May.

5.3. Model Improvements to Include Thermal Stress Estimations

Model simulation results for thermal stress estimations are shown in Figures 10-19. The thermal stress maps are provided for a hypothetical pavement test section at the hour when minimum pavement surface temperatures are predicted using Cheyenne, WY, typical meteorological year weather data. Six plots are provided for each simulation case described in the previous section: (1) hourly top and bottom slab surface temperatures for one year, (2) hourly top and bottom slab surface thermal stresses for one year for the *soft* pavement case (soft pavement is defined to have a stiffness modulus of about 150MPa at -40°C and an average modulus of elasticity of approximately 1300MPa or 190,000 psi), (3) hourly top and bottom slab surface thermal stresses for one year for the *typical* pavement case (a typical pavement is defined to have a stiffness modulus of about 550MPa at -40°C and an average modulus of elasticity of approximately 2500MPa or 360,000 psi), (4) temperature contours in pavement cross-section at the hour of maximum tensile stress, (5) thermal stress contours in pavement cross-section at the hour of maximum tensile stress for the *soft* pavement case, and (6) thermal stress contours in pavement cross-section at the hour of maximum tensile stress for the *typical* pavement case. Temperature dependency of stiffness modulus for both pavement types are given in Figure 4.

It was not possible to perform any reliable model validation due to the dearth of pavement temperature and corresponding tensile strength values due to the fact that fracturing temperature is quite location specific and strongly dependent on the bitumen content of the asphalt.

Nevertheless, some qualitative and semi-quantitative observations are possible from the simulation results presented in Figures 10 through 19. First, considering a tensile strength of asphalt of 0.5 MPa (Hills, 1974), the *soft* pavement would not experience cracking under the cold temperatures observed. Under the coldest surface temperature observed, which was –37^{o}C for Case 1, the stiffness modulus for the *soft* pavement was determined to be about 100 MPa. This is in agreement of Superpave recommendations of 300 MPa to prevent cracking.

On the contrary, the *typical* pavement was observed to crack under cold conditions in all cases simulated. Cracking would occur at temperatures of approximately –30^{o}C to –40^{o}C. At these temperatures, the stiffness modulus rises sharply with decreasing temperature from about 150 MPa at –30^{o}C to about 300 MPa at –35^{o}C. A significant observation from the simulation results is that the thermal stresses are considerably lower in higher thermal conductivity pavements (Figure 14). This is most likely due to the fact that increasing thermal conductivity results in smaller temperature changes due to improved heat transfer, and thus lower thermal stresses.

In the two-lane cases (Cases 3 and 4), planes of constant stress mimic the thermal conductivity of the pavement sections. In comparing the two-lane simulation results with the single-lane simulation results, it appears that the largest stress gradient as well as the largest stress values occur when a lower thermal conductivity layer is underlain by a higher thermal conductivity layer. This may be explained by considering the heat balance on a pavement slab. The driving energy potential on a pavement slab is the heat flux at the top surface. Heat will be more readily transferred through higher conductive zones. The overall heat flux is the same, regardless of the spatial distribution of the thermal conductivity, but it is this spatial distribution of thermal conductivity that governs the temperature distribution within the slab, and therefore the distribution of thermal stresses. Correspondingly, largest thermal stresses may be expected at the interfaces of pavement layers with the greatest differences in thermal conductivities.

Stipulating that cracking will occur at pavement locations where the thermal stresses are calculated to be above 0.5MPa, the following observations are made for the typical asphalt pavement:

1) If material properties of asphalt lifts are relatively similar (Base Case) thermal distribution becomes somewhat evenly distributed throughout the pavement slab. Cracking is expected to occur in the upper lift. However, cracking in the lower lift may not be observed depending on the thermal environmental conditions.
2) If materials properties of the lifts are dissimilar (Case 1), cracking is predicted to occur throughout the upper lift penetrating as deep as to the interface of the two lifts. A low thermal conductivity upper lift causes higher temperatures in the upper lift, leading to larger magnitudes of thermal stresses throughout the upper lift.
3) A high thermal conductivity upper lift leads to better heat transfer off the top surface of the pavement. This reduces the magnitude of thermal stresses. Although cracking is still observed under the conditions simulated (Figure 15 c), the depth of predicted crack penetration is smaller when compared to the Base Case and Case 1.
4) In two-lane simulations, it is appears inadvisable to select asphalt mixes that are dissimilar with respect to their thermal properties. Figure 17 c shows that the high thermal conductivity upper lift dissipates heat significantly better than the low thermal conductivity upper lift. This causes higher temperatures and thermal stresses in the low thermal conductivity lift. Thermal cracking is predicted throughout the low thermal conductivity lift penetrating into the lower lift. Thermal

cracking predicted in the high thermal conductivity lift is somewhat significant near the horizontal interface. The depth of thermal stress cracking is confined to the top few centimeters.

5) When a two-lane asphalt segment is overlain with a single lift (Case 4), low thermal conductivity lower lift experiences significantly less thermal stress than the lane with high thermal conductivity. In the low thermal conductivity lower lift no cracking is predicted as cracking appears to be confined to the upper lift above the interface of the lifts.

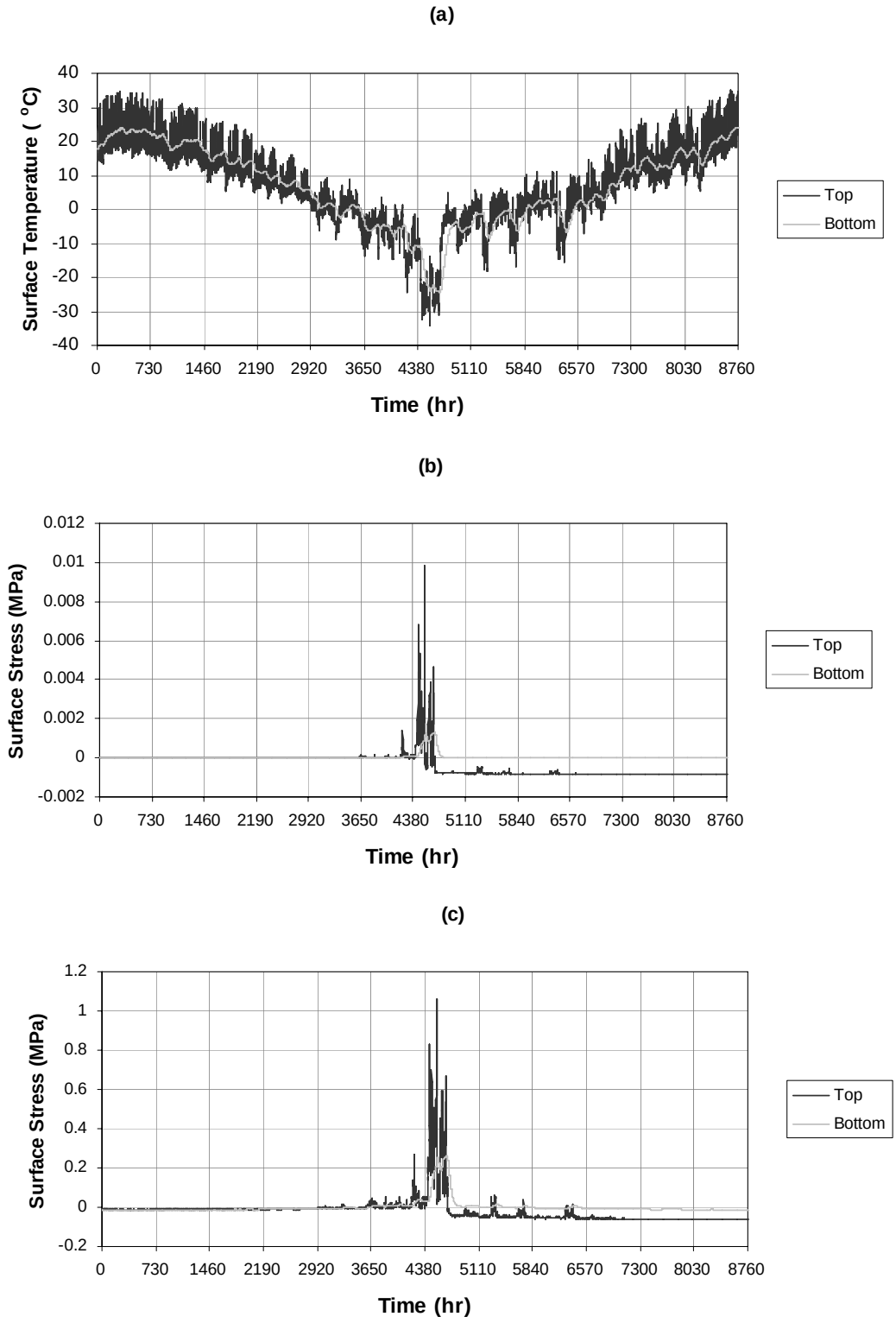

Figure 10. Base case slab **(a)** surface temperatures, **(b)** stresses for soft pavement, and **(c)** stresses for typical pavement. Note tensile stresses are positive, time 0 is July 1.

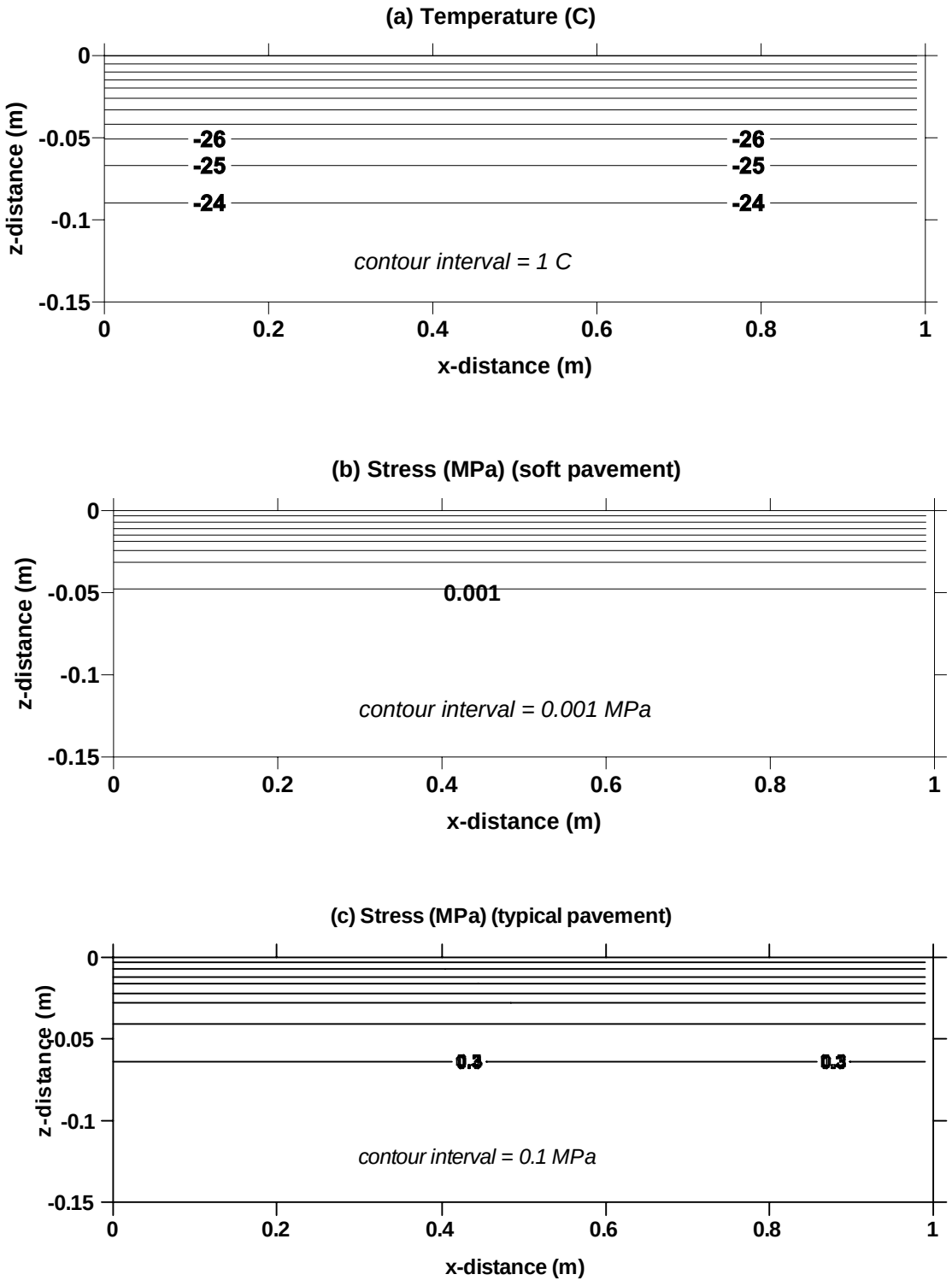

Figure 11. Base case pavement temperature and stress contour maps at maximum tensile stress.

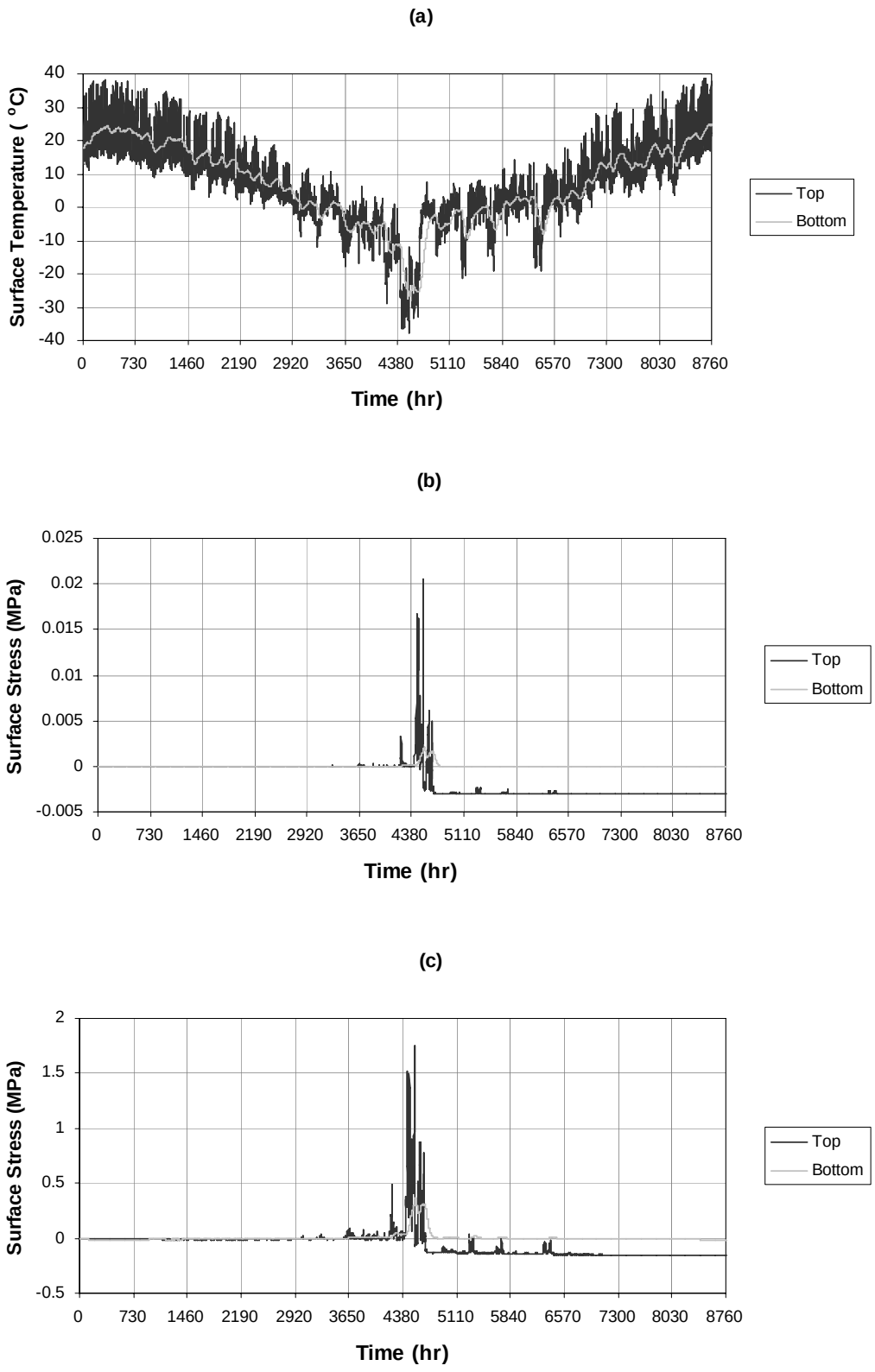

Figure 12. Low thermal conductivity surface case slab (Case 1) **(a)** surface temperatures, **(b)** stresses for soft pavement, and **(c)** stresses for typical. Note tensile stresses are positive, time 0 is July 1.

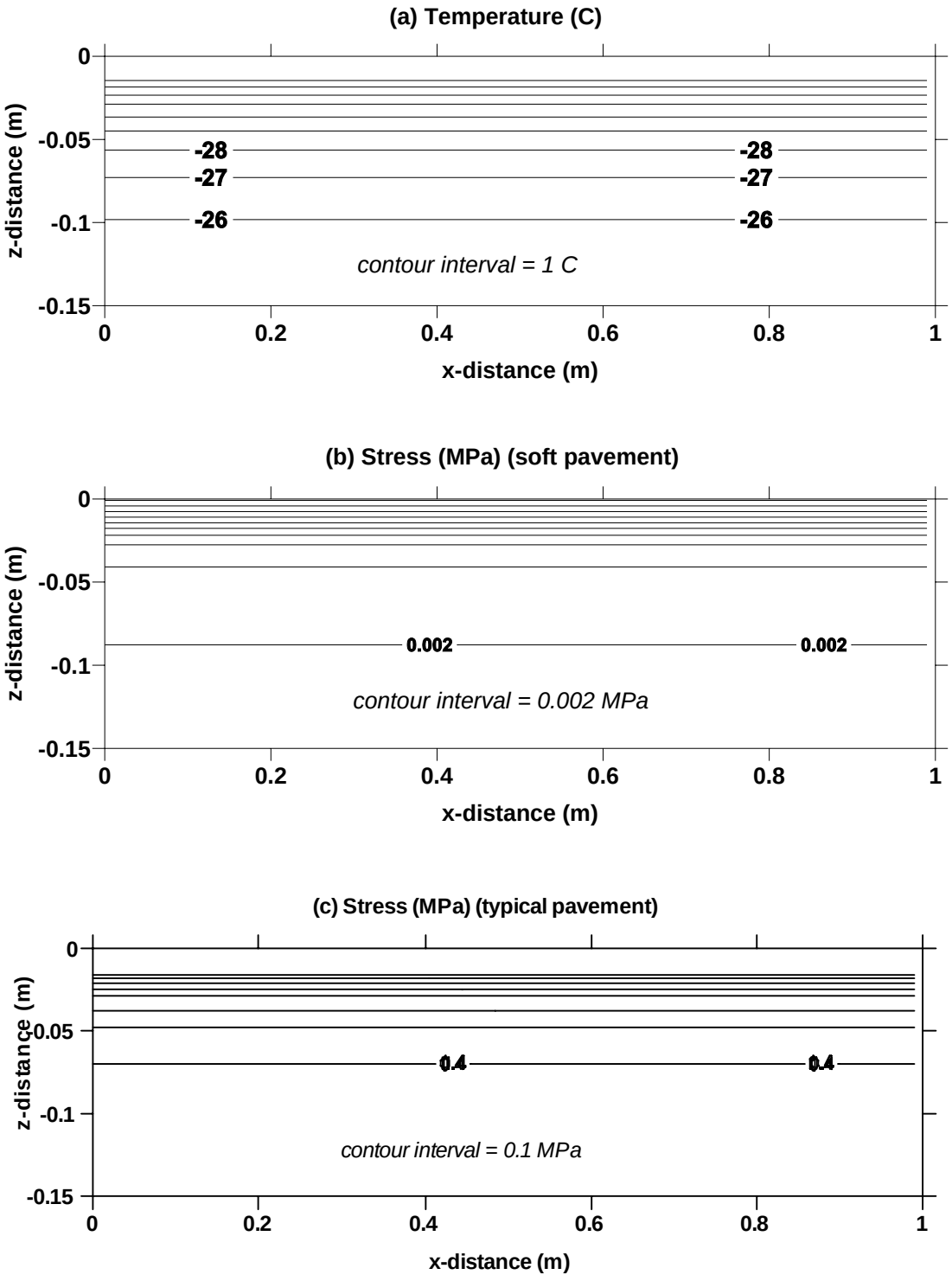

Figure 13. Low thermal conductivity surface case slab (Case 1) pavement temperature and stress contour maps at maximum tensile stress.

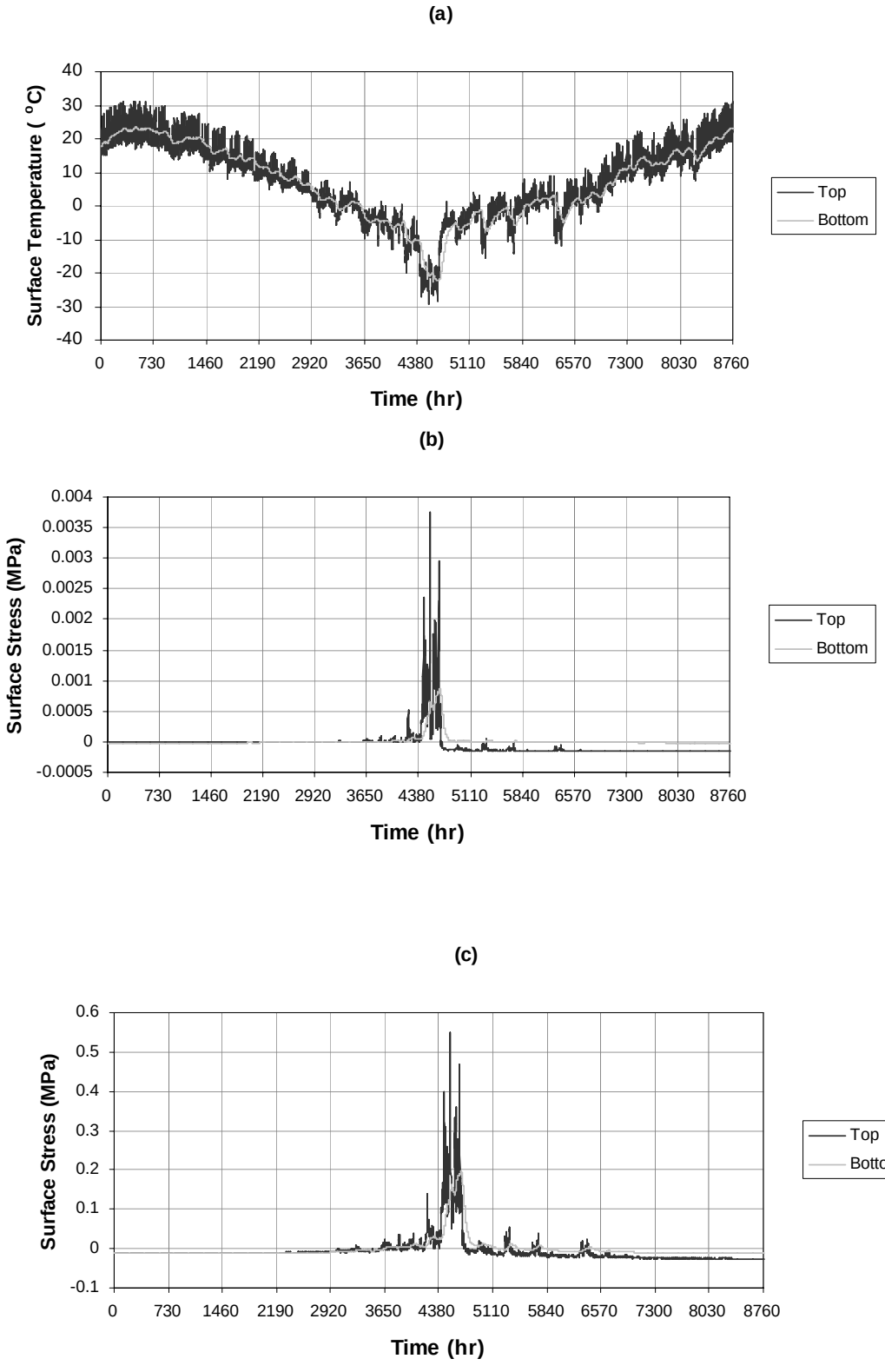

Figure 14. High thermal conductivity surface case slab (Case 2) **(a)** surface temperatures, **(b)** stresses for soft pavement, and **(c)** stresses for typical pavement. Note tensile stresses are positive, time 0 is July 1.

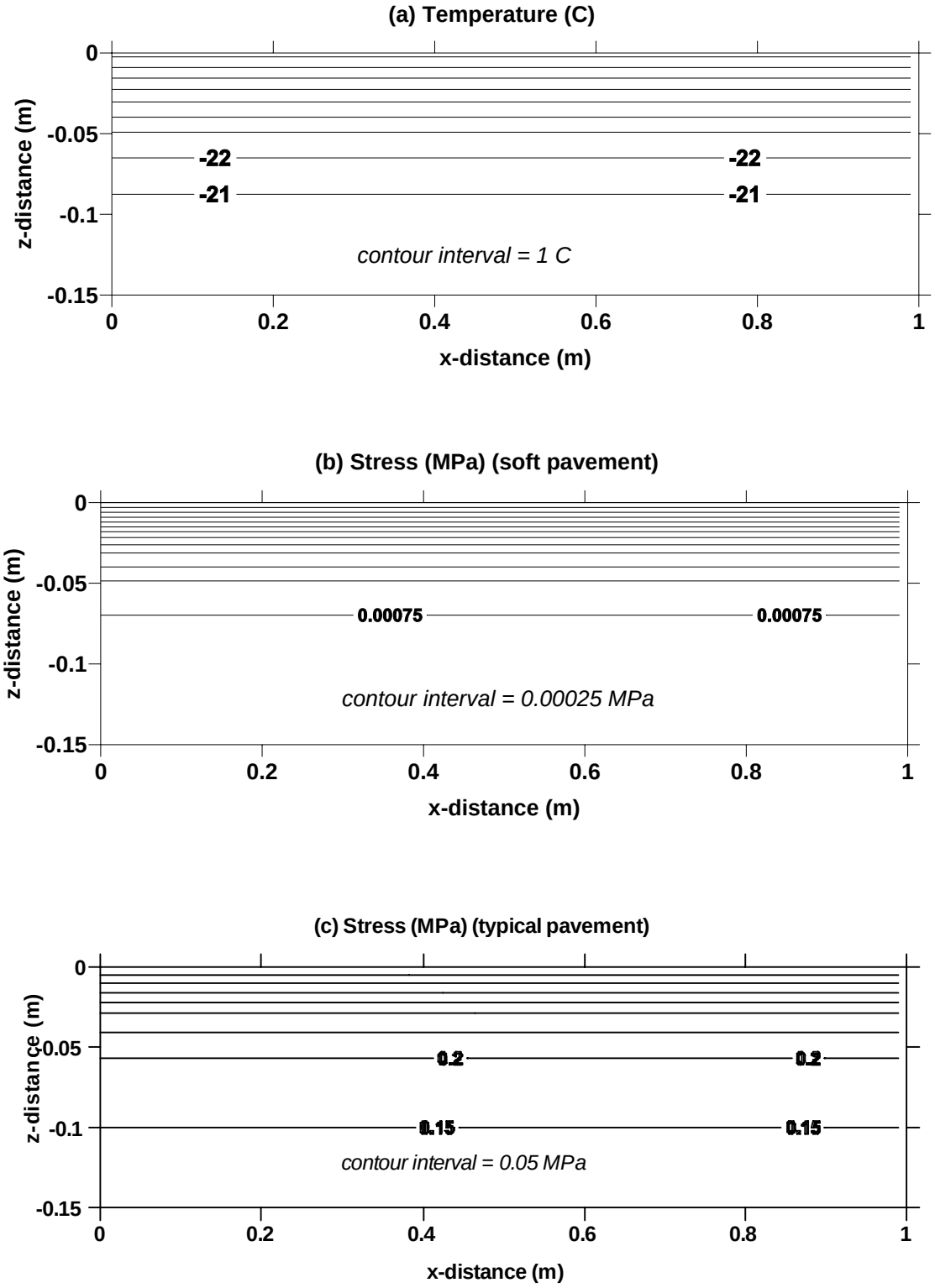

Figure 15. High thermal conductivity surface case slab (Case 2) pavement temperature and stress contour maps at maximum tensile stress.

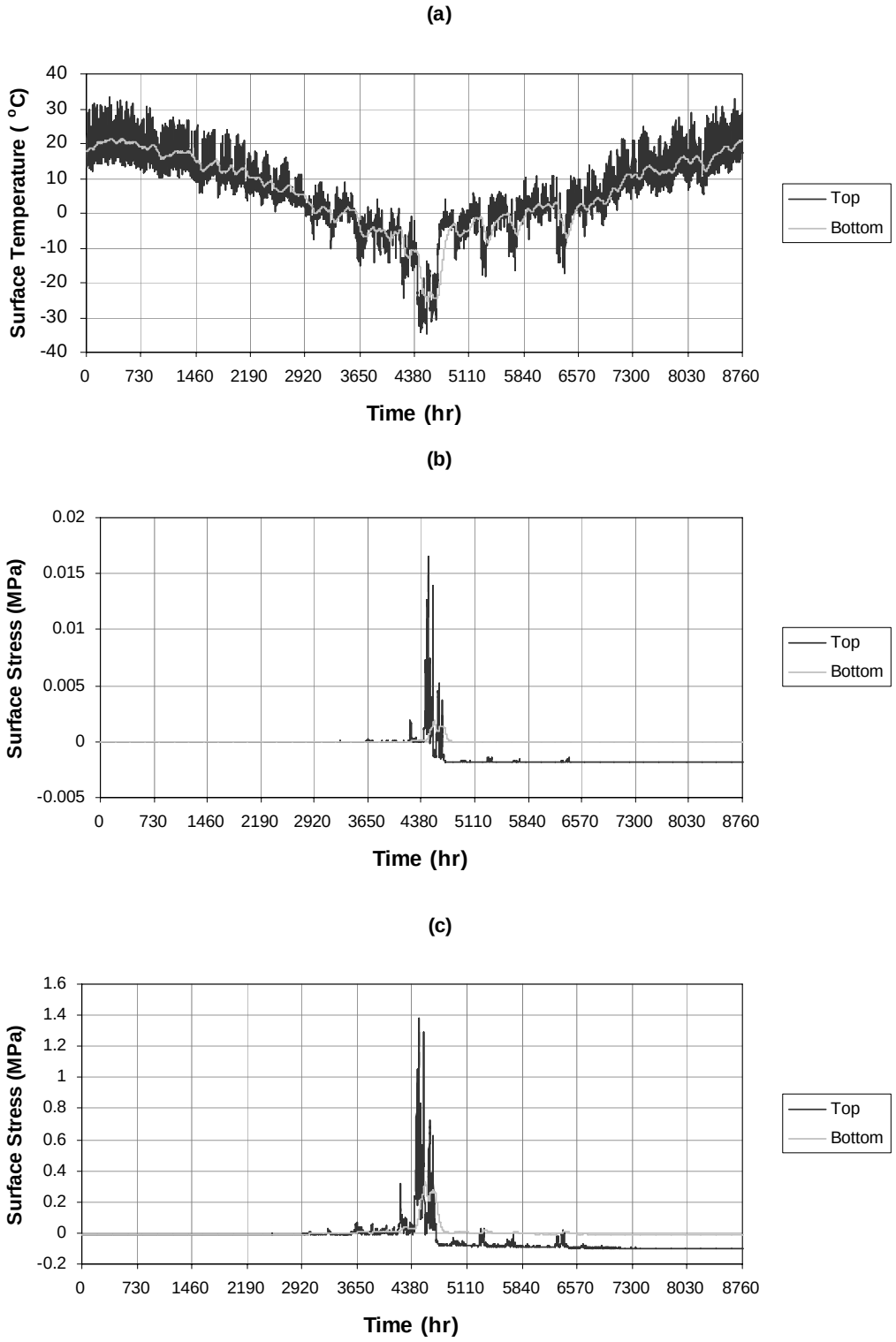

Figure 16. Two-lane slab (Case 3) **(a)** surface temperatures, **(b)** stresses for soft pavement, and **(c)** stresses for typical pavement. Note tensile stresses are positive, time 0 is July 1.

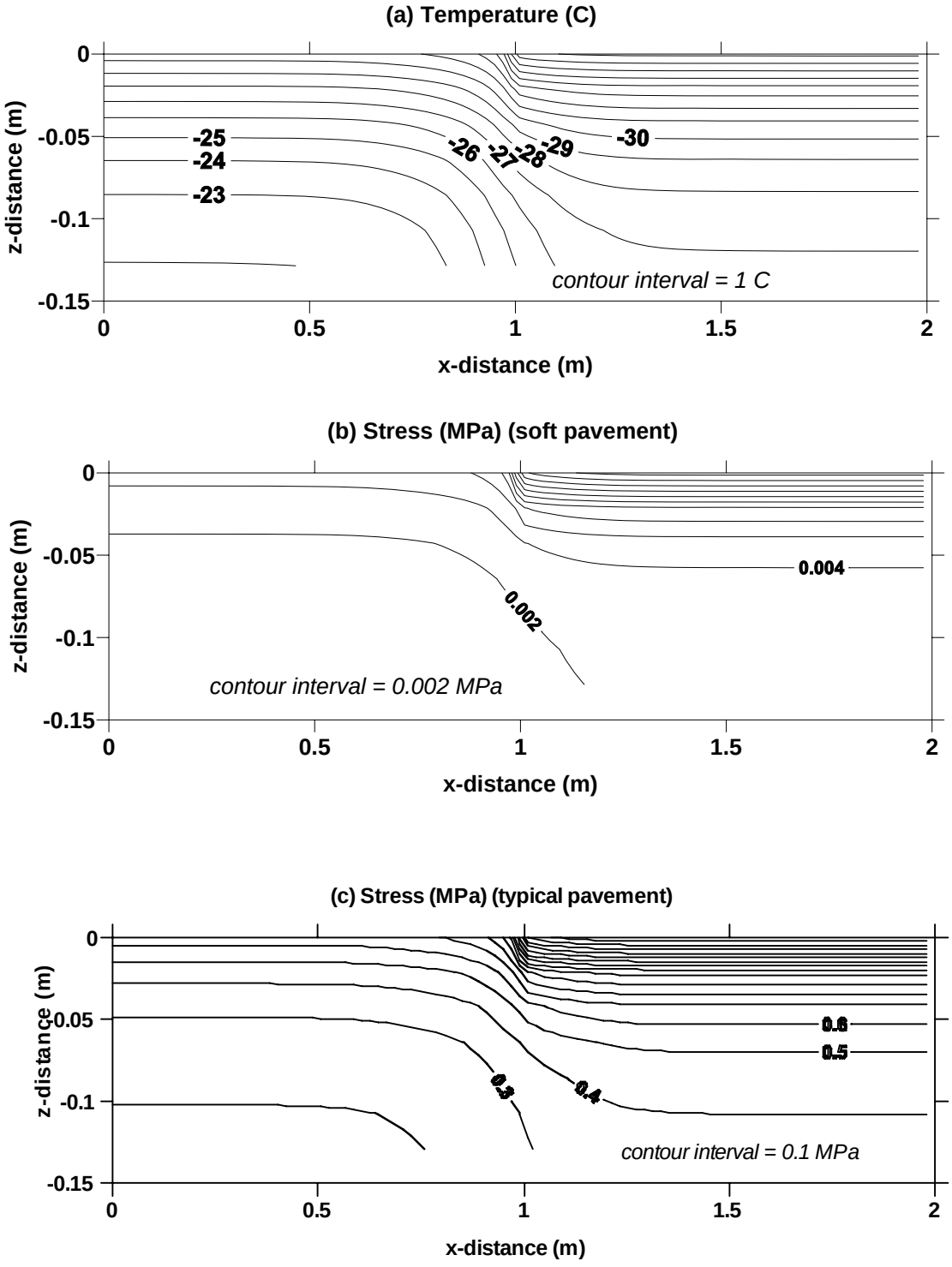

Figure 17. Two-lane slab (Case 3) pavement temperature and stress contour maps at maximum tensile stress.

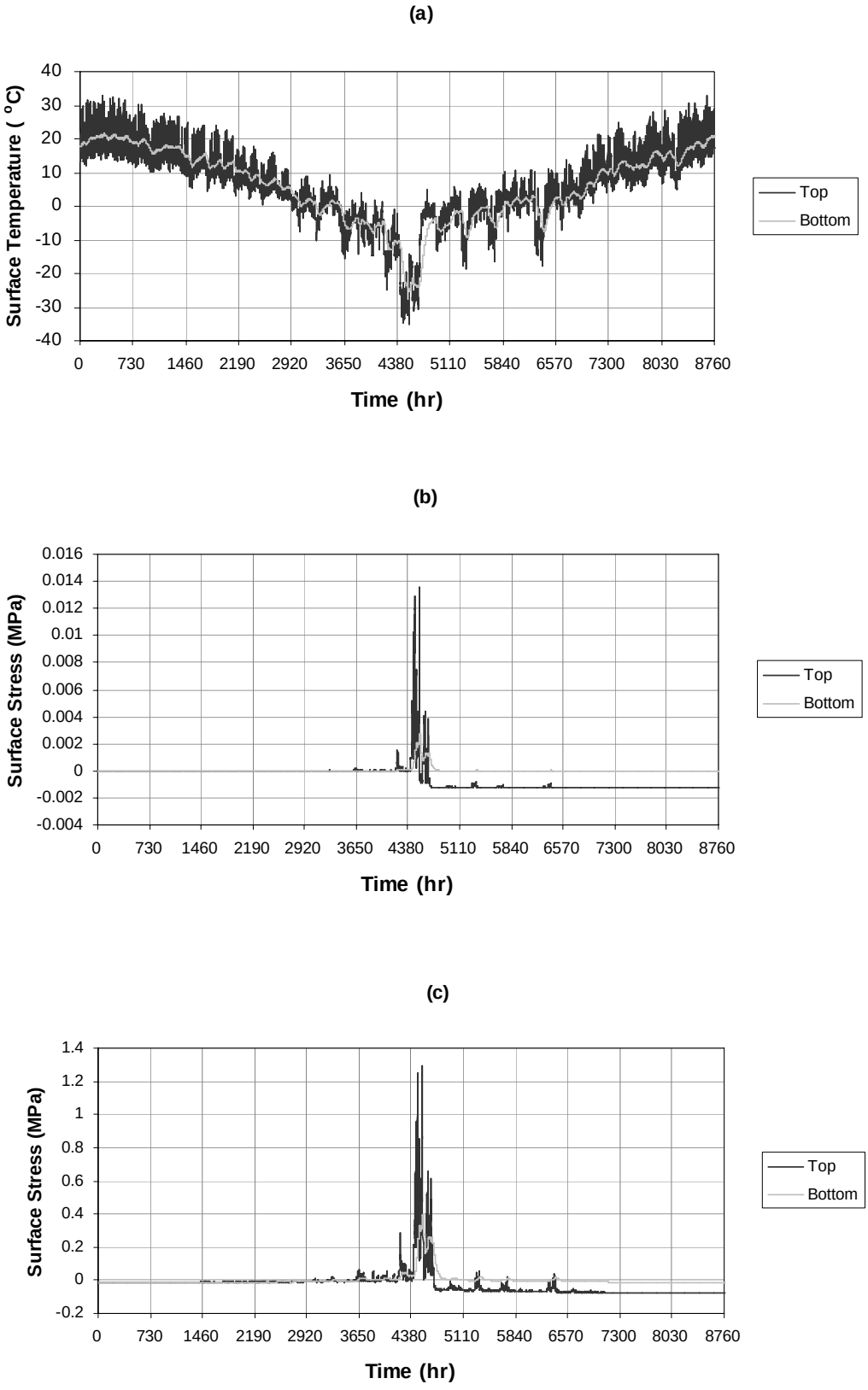

Figure 18. Two-lane slab (Case 4) **(a)** surface temperatures, **(b)** stresses for soft pavement, and **(c)** stresses for typical pavement. Note tensile stresses are positive, time 0 is July 1.

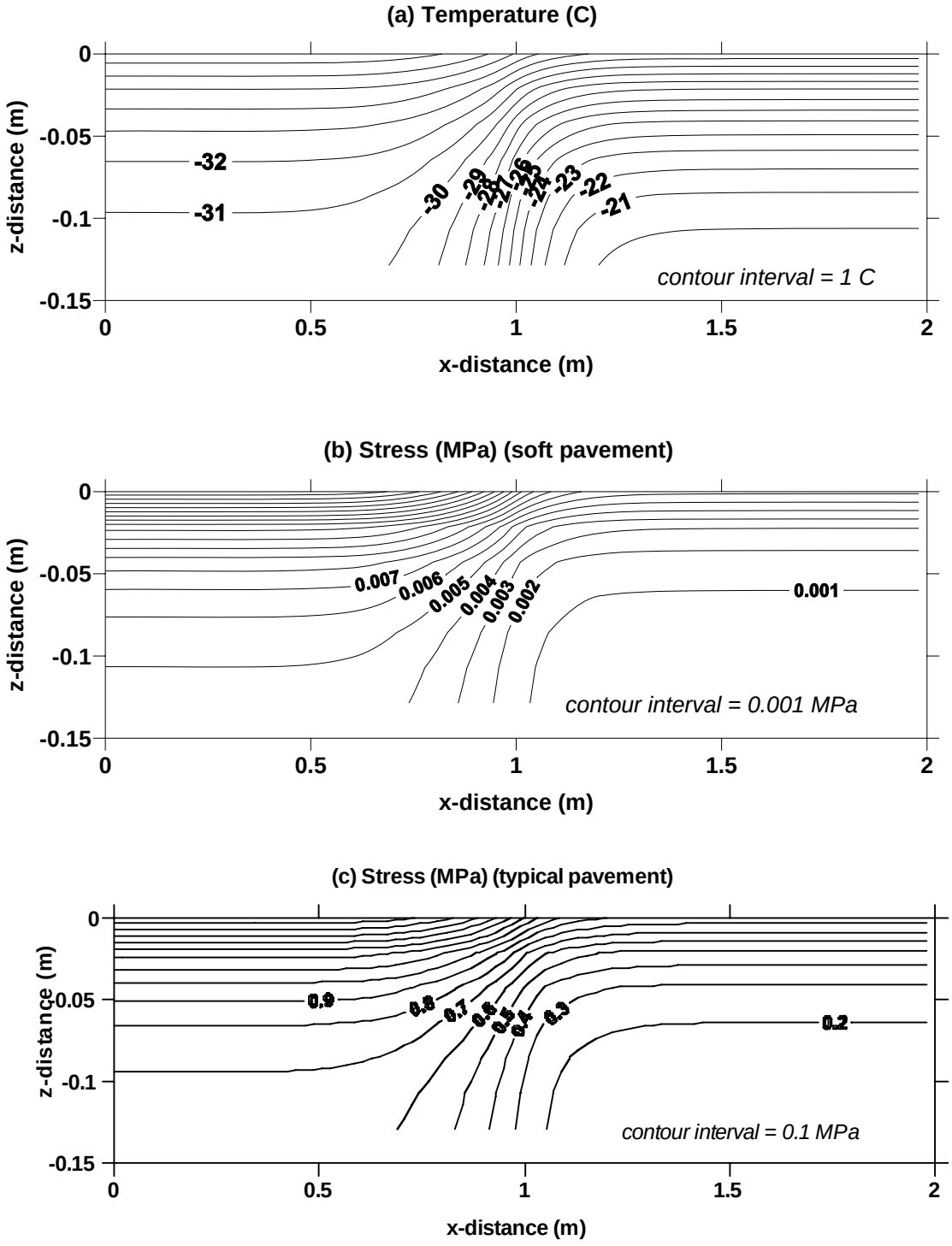

Figure 19. Two-lane slab (Case 4) pavement temperature and stress contour maps at maximum tensile stress.

6. CONCLUSIONS

An improved two-dimensional finite difference model is presented that is capable of determining the temperatures and thermally induced stresses on an hour-by-hour basis at any arbitrary point in an asphalt pavement. The model considers thermal ambient conditions such as the ambient dry bulb temperature, global solar radiation intensity, detailed pavement geometry and orientation, ambient wind conditions, effects of precipitation and pavement thermal properties. Following conclusions may be drawn from the analyses presented:

(1) The numerical model presented provides a powerful tool in determining pavement thermal behavior. The model allows for an hour-by-hour calculation of the pavement thermal response in the form of pavement temperatures and stresses using primary weather data for varying asphalt materials. The various lifts of asphalt materials can be entered into the model approximating layer geometry in 25mm grid increments in the direction normal to the asphalt surface through specification of thermal properties of asphalt materials (thermal conductivity, volumetric specific heat capacity and emissivity). This allows for the determination of temperature responses and thermal stresses at different lifts. In addition, the model allows for the specification of different asphalt materials in the horizontal direction. Thus, it is possible to define varying materials in each highway lane as well as in different lifts. This is a significant improvement over Superpave algorithms that were developed using analytical curve fitting techniques based on observed asphalt performance data.
(2) The numerical model predictions (temperatures and thermal stresses) are strongly dependent on climate data in addition to accurate knowledge of the thermal properties of pavement materials and pavement geometry.
(3) Pavement tilt angle can have a significant impact on top surface temperature. Depending on the surface azimuth, temperatures on a tilted surface will be seasonally higher or lower than temperatures on a horizontal surface.
(4) Precipitation and evaporation have a significant cooling effect on the pavement surface temperatures.
(5) Thermal stresses in asphalt pavements are significantly impacted by the thermal properties of pavement materials, specifically the thermal conductivity of asphalt layers. From the simulation results, it was observed that lower thermal stresses occur in the pavement when higher thermal conductivity layers are placed at the pavement top surface.

For the stress estimation model to be of practical use, stiffness modulii and tensile stresses of the asphalt must be known. These data are highly sample-specific, strongly depending on the bitumen content of the asphalt, and are difficult to obtain. In some cases, it may not be practical to measure these parameters, and therefore the model results are only as good as the estimates of the parameters.

7. RECOMMENDATIONS FOR FURTHER WORK

The following recommendations are made for further research in order to improve numerical model predictions to determine the maximum and minimum asphalt temperatures using local typical meteorological year weather data. Note that a number of the recommendations made in phase I of this project (Yavuzturk and Ksaibati, 2002) are reinforced below:

1) Further improvements to the two-dimensional numerical model are of interest through additional field validations using high quality weather and pavement data. This may be accomplished through a specially designed and instrumented pavement segment with a fully dedicated weather station nearby that would reflect the true ambient thermal conditions the pavement is exposed to. A dedicated weather station coupled with a specially designed test segment would allow for a more reliable field validation of pavement temperature and thermal stress predictions.
2) The numerical model may be further expanded to apply to pavements on bridge decks where an adiabatic bottom surface cannot be assumed due to convective cooling of the exposed bottom of the bridge deck. This convective cooling is primarily responsible for bridge deck icing during seasons when low ambient air temperatures are encountered along with high wind conditions.
3) The two-dimensional finite difference model may be expanded to the third dimension so that temperature changes can be assessed between pavement segments along the length of the pavement. A three-dimensional modeling would also allow for the accurate assessment of pavements including pavement thermal responses at bankments and slopes.
4) In cold climates, the effects of snow cover and freezing rain on pavement surfaces as well as freezing inside the asphalt material due to water seepage (varying moisture content of the pavement slab) impact the maximum and minimum asphalt temperatures considerably. The snow cover typically has an insulating effect on the surface reducing the amount of convective heat losses through the pavement. Although a significant step has been taken with this research to assess thermally induced stresses in pavements, the numerical model may be further expanded to include the effects of snow and mushy zones for a more realistic prediction of pavement temperatures allowing for more accurate and reliable pavement designs.
5) A graphical user interface that utilizes Windows programming techniques may be of interest for easy use by field engineers so that changes can be entered by the user on-the-fly without reliance on special programming tools.

8. REFERENCES AND BIBLIOGRAPHY

Adkins, D.F. and G.P. Merkley. 1990. Mathematical model of temperature changes in concrete pavements. *Journal of Transportation Engineering*, 116, 3: 349-358.

Anderson, D.A., L. Lapalu, M.O. Marasteanu, Y.M. Le Hir, J.P. Planche, and D. Martin. 2001. Low-temperature thermal cracking of asphalt binders as ranked by strength and fracture properties. *Transportation Research Record*, 1766: 1-6.

Ali, H.A. and A. Lopez. 1996. Statistical analyses of temperature and moisture effects on pavement structural properties based on seasonal monitoring data. *Transportation Research Record*, 1540: 48-55.

ASHRAE, 2001. *ASHRAE Handbook, Fundamantals*. American Society of Heating, Refrigeration and Air-Conditioning Engineers, Inc., Atlanta, GA.

van Bijsterveld, W.T., L.J.M. Houben, A. Scarpas, and A.A.A. Molenaar. 2001. Using pavement as solar collector – effect on pavement temperature and structural response. *Transportation Research Record*, 1778: 140-148.

Branco, F.A. and P.A. Mendes. 1993. Thermal actions for concrete bridge design. *Journal of Structural Engineering*, 119, 8: 2313-2331.

Boutin, G. and C. Lupien, 2000. Thermal Cracking of Asphalt Pavement. *Proceedings of the 2nd Eurasphalt & Eurobitume Congress*, Barcelona, Book II, pp. 45-59.

Bouzoubaa, N, M. Lachemi, B.Miao, and P.C. Aitcin. 1997. Thermal damage of mass concrete: experimental and numerical studies on the effect of external temperature variations. *Canadian Journal of Civil Engineering*, 24: 649-657.

Bliss, R.W., 1961. Atmospheric Radiation Near the Surface of the Ground. *Solar Energy*, 5(103).

Chandra, D., K.M. Chua, and R.L. Lytton. 1989. Effect of temperature on the load response of granular base course material in thin pavements. *Transportation Research Record*, 1252: 33-41.

Choubane, B. and M. Tia. 1995. Analysis and verification of thermal-gradient effects on concrete pavement. *Journal of Transportation Engineering*, 121, 1: 75-81.

Deacon, J.A., J.S. Coplantz, A.A. Tayebali, and C.L. Monismith. 1994. Temperature considerations in asphalt-aggregate mixture analysis and design. *Transportation Research Record*, 1454: 97-112.

Duffie, J.A. and W.A. Beckman, 1991. *Solar Engineering of Thermal Processes, 2nd Edition*. John Wiley and Sons.

Harik, I.E., P. Jianping, H. Southgate, and D. Allen. 1994. Temperature effects on rigid pavements. *Journal of Transportation Engineering*, 120, 1: 127-143.

Hermansson, A. 2000. Simulation model for calculating pavement temperature including maximum temperature. *Transportation Research Record*, 1699: 134-141.

Hermansson, A. 2001. Mathematical model for calculation of pavement temperatures. *Transportation Research Record*, 1764: 180-188.

Hills, J.F., 1974. Predicting the fracture of asphalt mixes by thermal stress. *Institute of Petroleum.*.

Inge, E.H. and Y.R. Kim. 1995. Prediction of effective asphalt layer temperature. *Transportation Research Record*, 1473: 93-100.

Irvine, T.F. Jr. and Liley, P.E., 1984, Steam and Gas Tables with Computer Equations, Academic Press, Inc.

Ioannides, A.M. and L. Khazanovich. 1998. Nonlinear temperature effects on multilayered concrete pavements. *Journal of Transportation Engineering*, 124, 2: 128-136.

Jung, D. and T.S. Vinson. 1993. Thermal stress restrained specimen test to evaluate low-temperature cracking of asphalt-aggregate mixtures. *Transportation Research Record*, 1417

Kapila, D., J. Falkowsky, and J.L. Plawsky. 1997. Thermal effects during the curing of concrete pavements. *ACI Materials Journal*, 94, 2: 119-128.

Kim, N. R. Roque, and D. Hiltunen. 1994. Effect of moisture on low-temperature asphalt mixture properties and thermal-cracking performance of pavements. *Transportation Research Record*, 1454: 82-88.

Kuo, C.M. 1998. Effective temperature differential in concrete pavements. *Journal of Transportation Engineering*, 124, 2: 112-116.

Liang, R.Y. and Y.Z. Niu. 1998. Temperature and curling stress in concrete pavements: analytical solutions. *Journal of Transportation Engineering*, 124, 1: 91-100.

Liao, C.J. and T.D. Hogue. 1996. *Thermal stress predictions for geothermally heated bridge decks*. Oklahoma State University; prepared for State of Oklahoma, Department of Transportation, 44 p.

Marrero, T.R. and E.A.Mason, 1972. Gaseous Diffusion Coefficients. *Journal of Physical and Chemical Reference Data*. 1: 3-118.

Marshall, C., R. Meier, M. Welch. 2001. Seasonal temperature effects on flexible pavements in Tennessee. *Transportation Research Record*, 1764: 89-96.

Masad, E., R. Taha, and B. Muhunthan. 1996. Finite-element analysis of temperature effects on plain-jointed concrete pavements. *Journal of Transportation Engineering*, 122, 5: 388-398.

Mills, A.F., 1995. *Basic Heat and Mass Transfer*. Prentice Hall.

Nishizawa, T, S. Shimeno, A. Komatsubara, and M. Koyanagawa. 1998. Study on thermal stresses in continuously reinforced concrete pavement. *Transportation Research Record*, 1629: 99-107.

Pane, I., W. Hansen, and A.R. Mohamed. 1998. Three-dimensional finite element study on effects of nonlinear temperature gradients in concrete pavements. *Transportation Research Record*, 1629: 58-66.

Park, D.Y., N. Buch, and K. Chatti. 2001. Effective layer temperature prediction model and temperature correction via falling weight deflectometer deflections. *Transportation Research Record*, 1764: 97-111.

Raad, L., S. Saboundjian, P. Sebaaly, and J. Epps. 1998. Thermal cracking models for AC and modified mixes in Alaska. *Transportation Research Record*, 1629: 117-126.

Rao, D.S.P. 1986. Temperature distributions and stresses in concrete bridges. *ACI Journal*, 83, 4: 588-596.

Rees, S.J., J.D. Spitler, and X. Xiao. 2002. Transient analysis of snow-melting system performance. *ASHRAE Transactions*, 108, 2: 406-423.

Roeder, C.W. and Moorty, S. 1991. Thermal movements in bridges. *Transportation Research Record*, 1290: 135-143.

Schindler, A.K. and B. McCullough. 2002. Importance of concrete temperature control during concrete pavement construction in hot weather conditions. *Transportation Research Record*, 1813: 3-10.

Shalaby, A., A.O. Abd El Halim, and S.M. Easa. 1996. Low-temperature stresses and fracture analysis of asphalt overlays. *Transportation Research Record*, 1539: 132-139.

Shen, W and D.J. Kirkner, 2001. Thermal Cracking of Viscoelastic Asphalt-Concrete Pavement. *Journal of Engineering Mechanics*, Vol. 127, No. 7, pp.700-709.

Solaimanian, M. and T.W. Kennedy. 1993. Predicting maximum pavement surface temperature using maximum air temperature and hourly solar radiation. *Transportation Research Record*, 1417: 1-11.

Spencer, J.W., 1971. Fourier Series Representation of the Position of the Sun. *Search*, 2(5).

Stoffels, S.M., W.R. Lauritzen, and R. Roque. 1993. Temperature estimation for low-temperature cracking of asphalt concrete. *Transportation Research Record*, 1417: 158-167.

Tart, R.G. 2000. Pavement distress and roadway damage caused by subsurface moisture and freezing temperatures – case histories from Alaska. *Transportation Research Record*, 1709: 91-97.

Tinker, J.A. and J.G. Cabrera. 1992. Modeling the thermal conductivity of concrete based on its measured density and porosity. In *Thermal Performance of the Exterior Envelopes of Buildings V;* Proceedings of the ASHRAE/DOE/BTECC Conference, Clearwater Beach, FL: 91-95.

Yoder, E.J. and M.W. Witczak, 1975. *Principles of Pavement Design, 2nd Edition*. John Wiley and Sons.

Yu, H.T., L. Khazanovich, M.I. Darter, and A. Ardani. 1998. Analysis of concrete pavement responses to temperature and wheel loads measured from instrumented slabs. *Transportation Research Record*, 1639: 94-101.

Zuk, W. 1965. Thermal behavior of composite bridges – insulated and uninsulated. *Highway Research Record*, 76: 231-.